5
Basic Applications for Teaching: Direct Visualization of Physics Phenomena

5.1
Introduction

Infrared thermal imaging allows quantitative and qualitative imaging of a multitude of phenomena and processes in physics, technology, and industry. During the last decade, thermography has also started to become popular for physics teaching at universities since it allows visualization of phenomena dealing with minute energy transfer, for example, in processes involving friction, which cannot be easily demonstrated with other methods [1–4]. Therefore, in this chapter, the focus is on selected applications of qualitative IR imaging of phenomena for physics education. The examples are intended to inspire more experiments by demonstrating how IR imaging can be used in teaching physics and in visualizing fundamental principles and processes. Unfortunately, seemingly simple phenomena very often involve complex explanations. Therefore, despite the simplicity of the phenomena, a complete quantitative analysis is far beyond the scope of this chapter. The topics are arbitrarily divided into the classical categories of physics i.e., mechanics, thermal physics, electromagnetism, and optics, followed by radiation physics as an example for using thermography in ''modern physics.'' Of course, many other applications, which are treated in later chapters can and should also be used for physics teaching such as, for example, thermal reflections (Section 9.2), detection of gases (Chapter 7), building insulation (Chapter 6), heat sources in electrical components (Section 9.7), and so on. More details to the physics of the phenomena can be found in nearly every textbook on introductory physics (e.g., [5, 6]).

5.2
Mechanics: Transformation of Mechanical Energy into Heat

A very important field for IR imaging in physics education concerns the visualization of mechanical phenomena involving friction. The most important everyday phenomenon concerns our ability to move around. Walking, riding bicycles, motorbikes, or cars is only possible due to frictional forces between the shoes/tires on one hand and the floor/the street on the other hand. Whenever there is a force acting

Infrared Thermal Imaging. Michael Vollmer and Klaus-Peter Möllmann

ISBN: 978-3-527-40717-0

along a given direction for a given distance, work is done, which is finally converted into thermal energy (often briefly but not very precisely denoted as heat). For sliding friction, this will ultimately lead to a temperature rise of the two areas that are in contact. In contrast, static friction which is the physical basis for walking or driving on vehicles with wheels will not convert work into thermal energy. In these cases, a closer look will show that inelastic deformations of the two touching objects will, however, also produce heat, which can be made visible with IR imaging.

5.2.1 Sliding Friction and Weight

Whenever two dry unlubricated solid surfaces slide over each other, there are frictional forces, which can be expressed by the empirical law $F_{\text{friction}} = \mu \cdot F_{\text{normal}}$, where $\mu < 1$ is the coefficient of friction and F_{normal} is the normal force with which each surface presses onto the other (e.g., [5, 6]). One distinguishes coefficients for static friction μ_{static} (no movement yet) and for kinetic friction μ_{kinetic}, that is, after a sliding of the two surfaces has been realized. Some typical μ-values for sliding friction, for example, for wood on wood or a car tire on the pavement of a street are in the range of 0.5. If some object is, for example, sliding across the floor, work must be done against frictional forces. Imagine that after a while the objects have a constant sliding velocity. In this case, the work is only used to overcome the kinetic frictional forces. It is ultimately converted into thermal energy, that is, the temperature of the two sliding surfaces will rise.

In order to analyze these effects of frictional energy transfer in more detail, two different weights of 1 and 5 kg respectively, were placed on small wooden plates and drawn simultaneously with constant speed across the floor (Figure 5.1). The heavier weight led to a much larger warming of the floor as expected, since the normal force was increased by a factor of 5. The plate surfaces were also heated up (not shown here). This experiment qualitatively demonstrates the effects of

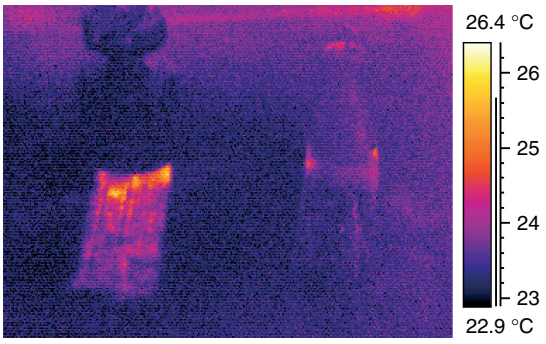

Figure 5.1 Two weights of 1 kg (right) and 5 kg (left) were placed on wooden plates and simultaneously drawn across the floor. The temperature rise of the floor is easily observed.

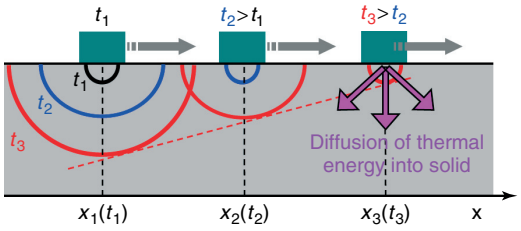

Figure 5.2 Transient thermal phenomena in sliding friction experiments arise from the fact that thermal energy diffuses into the bulk material, giving rise to spatial and time dependence of observable surface temperatures. The distance of energy diffusion into the bulk material as a function of time is indicated by the semicircles.

frictional forces in mechanics. A quantitative analysis would be quite complex. On one hand, it would require exact measurements of the frictional forces, and, on the other hand, the corresponding mechanical work would be split up into heating of both surfaces, depending on their thermal material properties. Finally, the diffusion of thermal energy from the directly heated contact surfaces would lead to transient effects, which means that a realistic modeling would require to record time sequences of this problem.

Figure 5.2 schematically illustrates (for the lower surface only) the transient effects of thermal energy diffusion into the bulk of the solid. It depicts a small object (blue–green) which is moving with constant speed across a solid surface. Three snapshots are shown at times t_1, t_2, and t_3 at which the object was at location x_1, x_2, and x_3 respectively. Owing to the work done by the object, the temperature at the contact spots rises to a maximum and then drops as a function of time due to first a lateral diffusion and second a diffusion of the energy into the bulk material. This transient behavior is characteristic for sliding friction phenomena.

Obviously, very simple looking basic physics phenomena become very difficult in a realistic quantitative analysis. This, however, is beyond the scope of this chapter, which only presents qualitative visualizations of physics phenomena.

5.2.2
Sliding Friction during Braking of Bicycles and Motorbikes

Very similar to the rising temperature of sliding planar surfaces as in the example above, the surfaces of bicycle, motor cycle, or automobile tires heat up during braking with blocked tires. The temperature of the contact spot of the tire with the pavement rises very quickly since the kinetic energy of the vehicle will be transferred into thermal energy. Figures 5.3 and 5.4 depict the temperature rise of the floor as well as of the tire for a bicycle after using the back pedal brake and for a motorbike on the road. For a motorbike braking from an initial velocity of 30 km h^{-1}, temperature rises can easily amount up to more than 100 K for the tire. The temperature rise of the floor again depends on the floor material, its

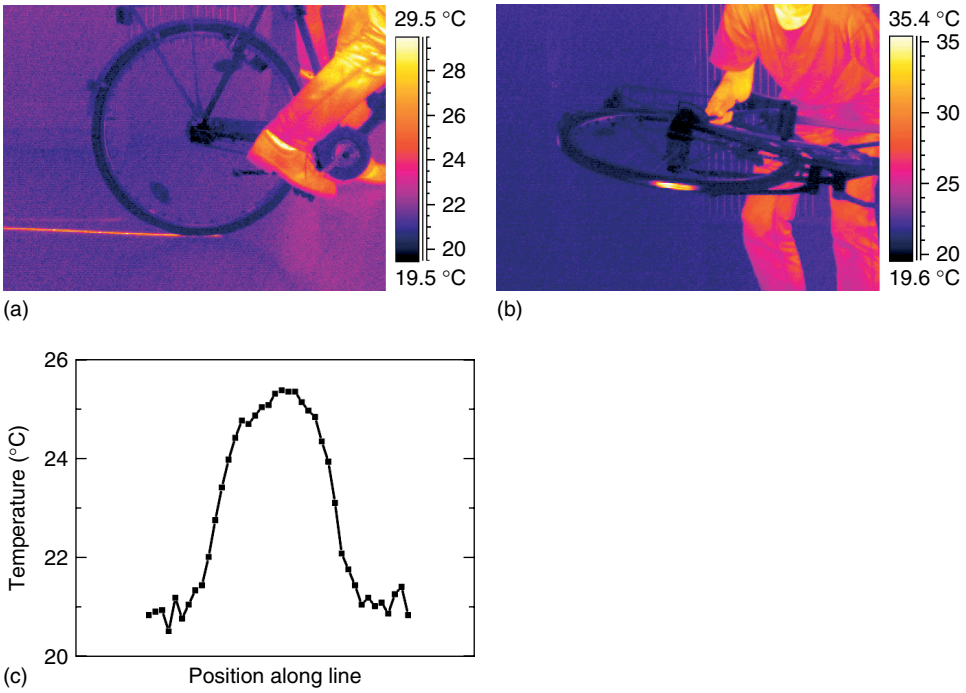

Figure 5.3 Sliding friction causes temperature rises during braking of a bicycle tire with a blocked wheel, using the back pedal brake (a,b). The heat transfer into adjacent locations on the floor is illustrated as temperature profile along a line perpendicular (c) to the trace on the floor, recorded several seconds after breaking.

thermal conductivity, heat capacity, and so on. It is usually smaller than the tire since the thermal energy is spread over a much larger area during the braking procedure. Figure 5.3c shows the temperature across the braking trace on the floor. It may be easily observed as a function of time, illustrating the transient thermal effects.

A very similar sliding friction phenomenon involves the use of the rim brakes. The contact between the friction pads (usually made of some kind of rubber) and the metal rim of the rotating wheel again uses sliding friction forces to transfer kinetic energy into thermal energy. Therefore, the rim itself as well as the friction pads can become very warm. Figure 5.5 depicts the wheel before and after a braking maneuver.

Braking maneuvers with blocked tires are not healthy for the tires. The hot spots on the tire go along with more material ablation at this location. This means that the lifetime of a tire will decrease for repeated braking maneuvers of this type

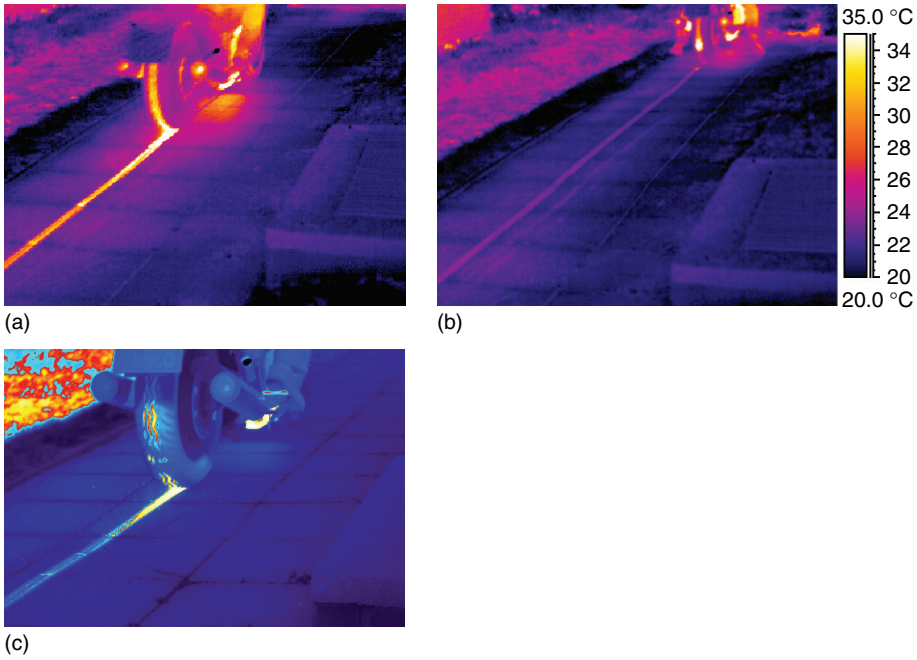

Figure 5.4 (a,b) Low-resolution LW camera image of the braking of a motorbike with blocked tires. The tire had a temperature reaching up to 100 °C immediately after stopping. (c) High-resolution image recorded with high-speed camera and smaller integration time.

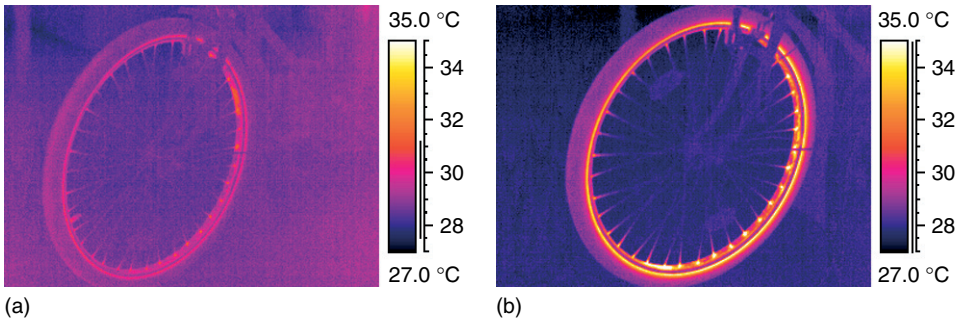

Figure 5.5 Sliding friction causes temperature rises during braking of a bicycle tire with a blocked wheel using the back pedal brake (a) and the rim brake (b).

(the same happens for "jackrabbit starts" where the accelerator pedal is pushed hard such that the wheels will skid leaving a similar black rubber trail behind as for braking with a blocked tire). In addition, the braking itself is not as efficient, since the coefficient of sliding friction is lower than the one for static friction. If sliding between tire and pavement is avoided, the slightly larger coefficient of static friction applies. In addition, during sliding, it is not possible to maneuver the car. For these reasons, modern cars are equipped with systems to prevent sliding friction during braking.

5.2.3
Sliding Friction: the Finger or Hammer Pencil

A very simple, but impressive demonstration of sliding friction and the corresponding temperature rises of surfaces is the use of a hammer or just a finger to write texts or equations on any convenient surface, for example, even the floor. The surfaces need not be too rough and their thermal conductivity should be not too large (in metals the thermal energy diffuses away very quickly, linoleum floors are excellent). Depending on finger speed and contact pressure, it is easily possible to achieve temperature differences of several Kelvin. Figure 5.6 depicts an example.

5.2.4
Inelastic Collisions: Tennis

Collisions are different mechanical phenomena that also involve energy transfer. One may think, for example, of two billiard balls, colliding with each other. Usually, one distinguishes elastic and inelastic collisions. Elastic collisions are those where the total kinetic energy of the objects before the collision is exactly equal to the total kinetic energy after the collision. Elastic collisions are idealized phenomena that are usually demonstrated in physics using apparatus to reduce any residual

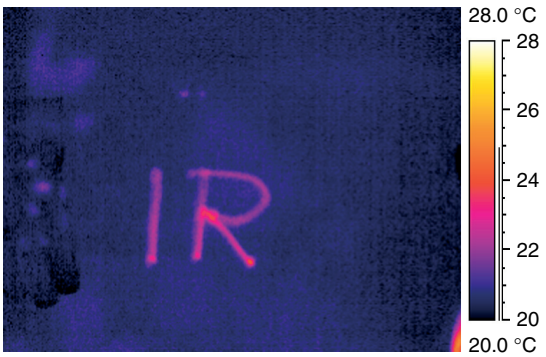

Figure 5.6 Finger writing: work against sliding frictional forces lead to temperature increase of the surface.

friction effects, for example, by using an air rail system. In practice, most collisions in everyday life are inelastic, that is, part of the kinetic energy of a moving object is transferred into thermal energy during the collision process. Think, for example, of any ball (tennis, soccer, volley ball, basket ball, rubber ball, etc.) which falls from a certain height to the floor. It will collide with the floor leading to a rebound. From energy conservation, an elastic collision of the ball with the floor would give the ball enough energy to reach its original height, from which it was dropped. However, no real ball will reach the original height from which it was dropped, that is, part of the initial kinetic energy is lost. For new tennis balls (mass $\approx$57 g, diameter $\approx$6.5 cm), it is required that if dropped from a height of 2.54 m, they must at least reach a rebound height of 1.35 m. This corresponds to a loss of kinetic energy of about 0.67 J, that is, about 47% of the initial kinetic energy is lost. Even super balls lose about 20% of their kinetic energy upon bouncing from a floor [7].

Microscopically, the ball as well as the surface deform upon impact of the ball. Consider, for example, the ball. If the deformation changes its shape from the ideal initial spherical shape to a distorted shape while touching the floor, it stores potential energy. Such deformations are, however, never totally elastic, that is, reversible, because during deformations part of the energy is transferred into thermal energy. This means that whenever we observe falling objects, colliding with surfaces, we expect temperature increases of the surface spot of the falling object as well as of the surface spot on the floor, where it hits. Figure 5.7 shows an example for an inelastic collision of a tennis ball with a floor.

In this experiment, where the ball was hit with a racket by an amateur, a temperature rise of the ball of about 5 K was observed with a decay time of several seconds. Similar to the friction experiment, a quantitative analysis is more difficult. The tennis ball experiment is explained in more detail in Section 10.3 when discussing high-speed thermography.

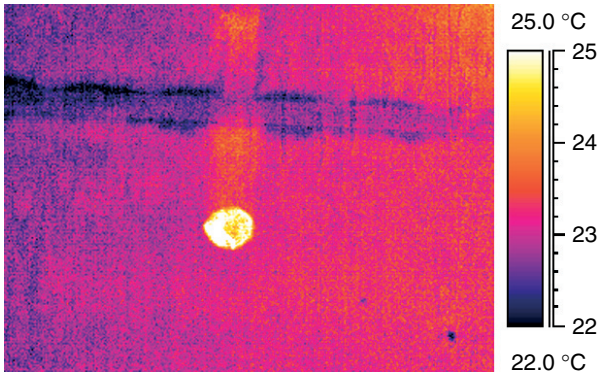

Figure 5.7 A tennis ball was hitting a carpet, resembling the court. The image was taken just after it touched the ground. The ball was also heated up during the collision, but – due to its fast movement – only left the vertical trace.

5.2.5
Inelastic Collisions: the Human Balance

If two objects stick together after a collision, it is termed as being *completely inelastic*. Imagine, for example, a piece of putty, falling to the floor. It will not rebound at all, that is, it loses all of its kinetic energy upon impact. The amount of energy transferred into thermal energy is larger than for inelastic collisions and therefore the corresponding temperature changes may be more easily observable. For the observation, it is however necessary to remove the object and turn it around after it has come to rest in order to measure the surface temperatures of the two contact areas.

Figure 5.8 shows an example of two persons of different mass $m_1 \approx 80$ kg and $m_2 \approx 120$ kg jumping down from a table to the floor. Both wear the same type of shoes. After landing, they quickly step aside and the contact spots on the floor are examined with IR imaging. Quite obviously, the heavier jumper gives rise to a higher surface temperature of the floor. One could easily argue that this was of course expected, since the heavier jumper started with a higher initial potential energy. This is correct, but again, a more thorough discussion shows that any kind of quantitative explanation will need much more information, for example, the contact area while hitting the floor maybe of different materials and hence different heat transfer properties of the soles of the shoes, and so on.

To elaborate, the two jumpers have different initial potential energies $m_i g h_i$ in the gravitational field of the earth, where h_i is the height difference between

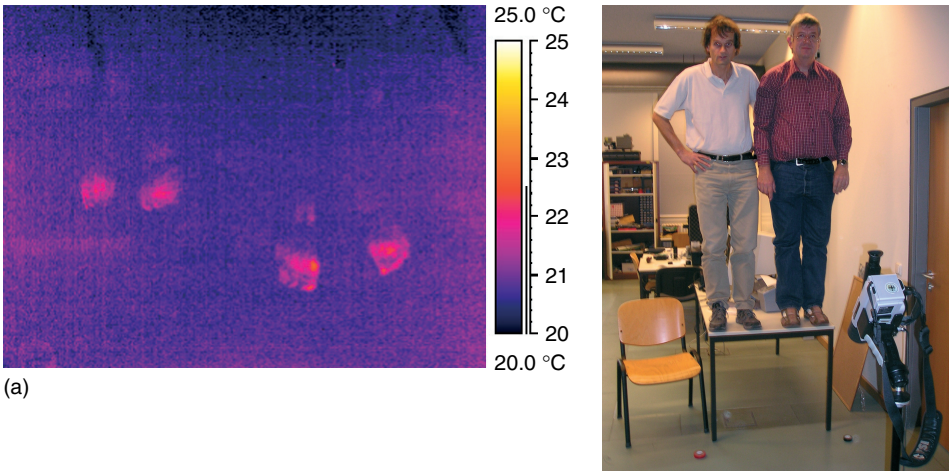

Figure 5.8 The human balance: The temperature rise due to an inelastic collision of people jumping from a table onto the floor (a) can be used to compare masses (weight forces) of the jumpers (b).

floor and center of gravity of the persons. In the following, we assume people of about the same height, $h_1 = h_2 = h$. Just before reaching the floor the potential energy has been completely transferred into kinetic energy $(1/2)\, m_i v_i^2$, where v denotes the velocity. During the completely inelastic collision, a first part of the kinetic energy is transferred into deformations of the floor and the shoes, a second part (i.e., the rest) into deformations within the body (muscles, knee joints, etc.). Ultimately, both parts will end up in thermal energy. Of course, it is only possible to measure the first part, that is, the temperature rise of the floor and the shoes with IR imaging. Unfortunately, again, the amount of energy dissipation within the body will depend on the jumper, that is, on the fact, whether and how muscles are stretched and it is not easily possible to guess the ratio of both contributions. Therefore, we assumed above that both jumpers try to jump in as similar a manner as possible, with muscles stretched. In this case, one expects that a similar ratio of energy would be dissipated into the shoe–floor contact area. It will then divide up into heating of the shoe and of the floor.

5.2.6
Temperature Rise of Floor and Feet while Walking

Walking on ice is very difficult, whereas walking on a dry street is easy. The difference between these two situations is that the frictional forces are much lower for the contact between shoes and ice as compared to that between shoes and pavement of a street. Obviously, friction is necessary for walking. However, although the phenomenon is one of the most natural for us, the details can become very complex. First, static friction is usually involved (the undesired sliding friction does apply to the ice, though). Usually there is no sliding between shoe and floor during walking. The shoe just touches the floor and then lifts up again. Since there is no distance traveled along the direction of an acting force, no mechanical work is done that could be converted into thermal energy.

The energetics of human walking and running has been studied in detail [8–10]. It involves work for accelerating and decelerating the legs plus the gravitational work associated with lifting the trunk at each step. The total power expended during walking finally leads to heating up of the body, sweating, and, to a small extent, also to a heating up of the two contact areas (this contribution has not been studied in detail so far; probably its portion of the total expenditure is at most in the percent-range, most likely in the single percent range). Microscopically, one may understand the mechanism for the heating from the inelastic collision experiment (Section 5.2.5). During each step, the shoe experiences something like an inelastic collision with the floor. Therefore, part of the original kinetic energy of the leg is transferred into deformation energy of the soles of the shoe as well as of the floor (and perhaps a small amount into the body of the walker). These deformation energies end up as thermal energy, that is, a temperature rise of the shoe and floor. How the total energy is split up depends again on the thermal properties of the two materials in contact.

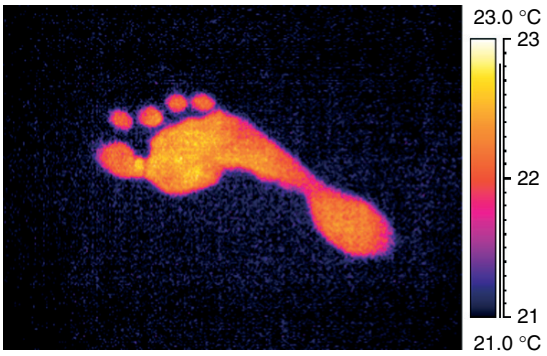

Figure 5.9 Energy dissipation due to walking can be visualized with IR imaging.

Figure 5.9 depicts an example of a person walking at constant speed with bare feet on a linoleum floor.

Since the foot hits the floor only with part of its surface, one easily sees the walking profile and the toes. The corresponding temperature rise is smaller for the shoes although still detectable, in particular when running, that is, hitting the floor with larger velocity (compare Figure 5.8).

5.2.7 Temperature Rise of Tires during Normal Driving of a Vehicle

Similar to walking, the driving of any vehicle with wheels is based on static frictional forces [7]. When a vehicle moves forward, its wheels rotate such that the bottom surface does not slide on the ground. Instead, a portion of the surface of each wheel touches the ground where it briefly experiences static friction. Then it moves up with a new portion of the wheel surface taking its place. This touch and release procedure involves only static friction; therefore, similar to the walking discussed above, this mechanism alone is not able to convert mechanical energy via work into thermal energy.

However, rolling of wheels on a surface involves more. The corresponding technical term for the resistance to motion is *rolling resistance* or *rolling friction*. Whenever a wheel or a tire rolls on a flat surface, it deforms the object as well as the surface. At the contact point/area, there are static frictional forces present. Sliding friction does not contribute since each contact spot on the tire is lifted up upon rolling. The deformation of the surface leads to reaction forces that have a component opposed to the direction of motion. As a matter of fact, the deformations of the surface lead to the seemingly paradox situation that any horizontally driving vehicle must drive upward (out of the hole due to the deformation).

As in the case of static and sliding friction, the frictional force is described as $F_{\text{friction}} = \mu_{\text{roll}} \cdot F_{\text{normal}}$ with μ_{roll} being the rolling friction coefficient. This coefficient is much smaller than typical static or dynamic friction coefficients, for

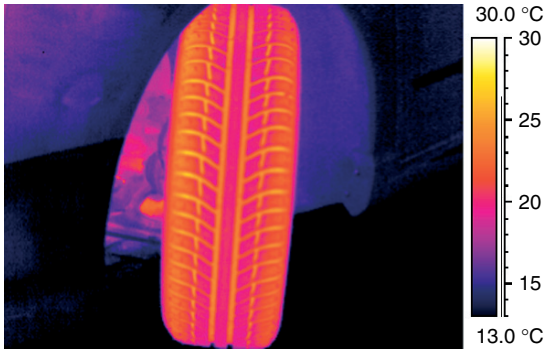

Figure 5.10 Homogeneous heating of tires during normal driving conditions. This is also a test of the quality of the profile of the tire; without profile, the heating would be more homogeneous across the tire surface.

railroad steel wheels on steel rails it is less than 0.001 and for car tires on asphalt about 0.03. Ideally, the deformations should be elastic, in which case, no thermal energy would be generated. In reality, part of the deformation is inelastic and the contact areas should warm up.

As a consequence, the tire of any transport vehicle will have elevated temperatures upon driving.

High-quality tires should have a homogeneously heated surface, provided that no braking with blocked tires or wheel spinning during accelerating contributes. Figure 5.10 depicts an example for a car. As expected, no hot spots are visible; however, the profile of the rather new tire is clearly visible.

This technique – investigation of tire surfaces after driving – is commonly used to analyze the quality of new tires, in particular of car tires for Formula One races.

5.3 Thermal Physics Phenomena

Although nearly all applications of IR imaging involve thermal phenomena, for example, by transferring mechanical or electrical energy into thermal energy and corresponding heating up of the surface of objects, there are some purely thermal physics phenomena which can be visualized using thermography. These include characteristic properties of heater systems, material properties like thermal conductivity, and also convection in liquids. IR imaging can be used to study the effect of phase transitions like in evaporative cooling or consequences of adiabatic processes like temperature differences due to adiabatic cooling. Finally, IR imaging offers possibilities for quantitative analysis of the heating and cooling of many objects.

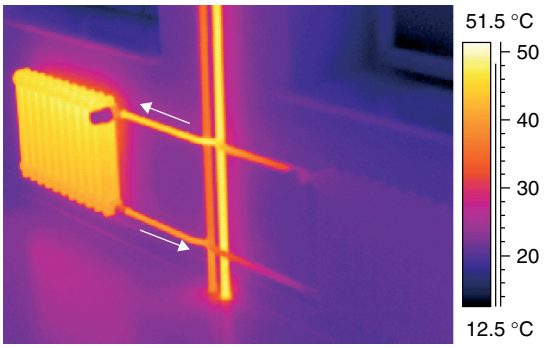

Figure 5.11 Radiator heater and water pipes with hot water (inflow) and slightly colder water (outflow).

5.3.1 Conventional Hot-Water-Filled Heaters

There are many indoor heating systems (e.g., wood, coal or oil stoves, or furnaces which use warm air heating or water-filled radiators) that can be analyzed with thermography. For physics teaching, it is very convenient to use hot water heaters whose hot water supply comes from a furnace. The hot water is usually driven by a pump and flows in pipes from room to room and, in each room, it also flows through the radiators, which transfer the heat to the room via convection and radiation.

Since the water is losing thermal energy to the heaters, it should be possible to detect a temperature difference between the inlet and outlet pipes of a radiator.

Figure 5.11 depicts a set of two radiator heaters in a lecture room close to the window as well as the vertical pipe system of inflow and outflow water. One of the heaters is turned on, the other is off. The image immediately visualizes the hot inlet water pipe and the slightly colder outlet water pipe. The water enters the radiator from top and slightly colder water flows out at the bottom as expected.

If IR image examples like these are shown when first introducing thermography, the confidence in the method increases. Probably many other well-known everyday life objects whose surface temperatures can also be measured separately with thermocouples can similarly build up confidence in this measurement technique.

5.3.2 Thermal Conductivities

In Section 4.2.1, conduction of heat was introduced as representing heat flow within a solid or fluid at rest, due to a temperature difference between its ends. The simplest theoretical system like a one-dimensional wall, which laterally extends indefinitely, can obviously not be measured with thermography. One needs to measure the surface temperature of objects.

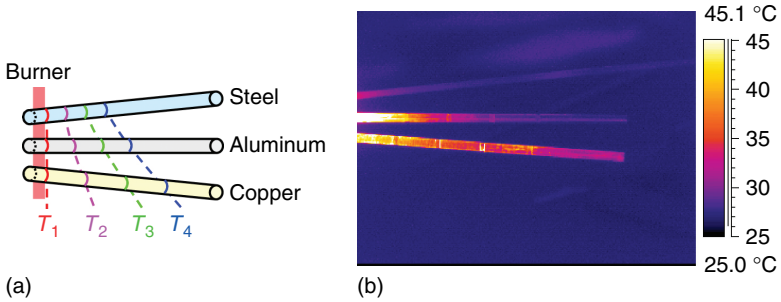

Figure 5.12 Typical setup of experiment to demonstrate thermal conductivity differences of materials (a). After heating has started the diffusion of heat into the rods proceeds with different velocities as indicated by the locations of the same temperature along the rods. (b) IR image of such a setup of steel, aluminum and copper rods, heated from one end (not seen in image) with a Bunsen burner.

A typical setup to demonstrate differences in thermal conductivity of solid materials is the following (Figure 5.12). Thin rods of different materials are horizontally fixed in such a way that one of their ends is free and the other end is heated (e.g., by flames of a Bunsen burner). Along the length of the rods, small pieces of wax can be attached at regular intervals (not shown in figure). The wax starts to melt at a certain temperature. Therefore, melting indicates that the critical temperature has been reached. The experiment is done by recording the times at which wax at given locations starts to melt. This allows visualization of the heat diffusion within the rods as a function of time. In particular, at a given distance from the heating location, the wax will start to melt earlier for rods with higher thermal conductivity. This experiment, nicely, but only qualitatively, demonstrates thermal conductivity. Unfortunately, it is not thermal conductivity alone that determines the outcome of such an experiment. First, for any quantitative analysis of thermal conductivity, a well-defined temperature difference is needed. Since, however, the rod ends are usually not fixed in a heat bath, but just end in air at room temperature, the whole rod will start to warm up and the end temperature will also increase with time. Second, convective heat losses due to the surface area of the rods and, third, the radiation losses will also contribute. As a consequence, it may well be that if these additional losses dominate, the temperature profile would not allow any precise conclusion concerning the thermal conductivity.

Figure 5.12 also depicts an IR image of such an experiment. Three rods of the same diameter, made of steel (top), aluminum (middle), and copper (bottom) were heated at one end using a flat flame Bunsen burner. The thermal conductivities (Table 4.1) increase from top to bottom. As expected, the Cu rod with the largest thermal conductivity is heated up much more quickly than steel and Al. In order to avoid saturation of the IR detectors close to the heating zone, it is best to first heat and then record images directly after turning off the heater.

A more well-defined setup for thermal conductivity measurements uses a fixed temperature difference between the two ends of a material, here water. A particularly

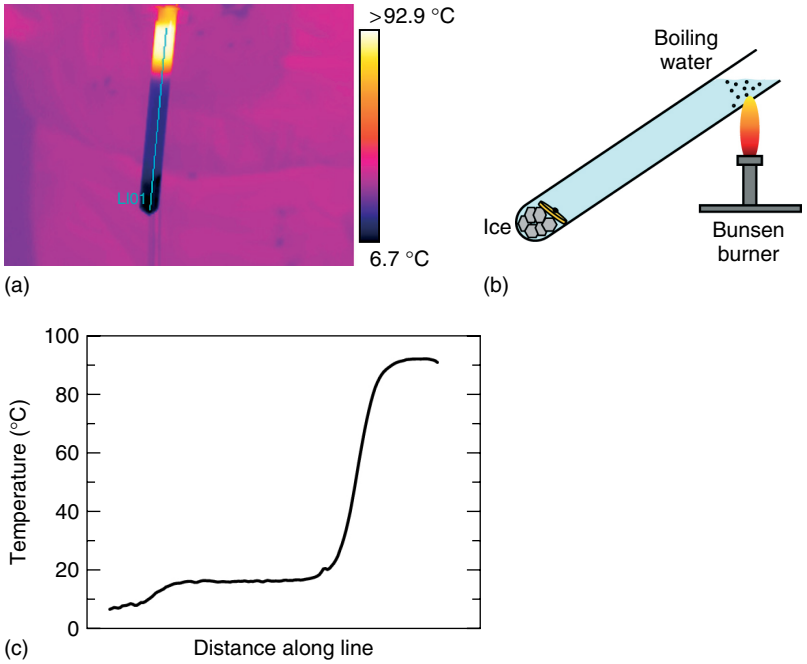

Figure 5.13 (a) IR image and setup for demonstration of thermal conduction in water. (b) Line plot of temperature reveals ice water at the bottom while the water at the top, recorded directly after turning off the burner, is still around 90 °C.

simple experiment is depicted in Figure 5.13. An ice cube is crushed and some pieces are put into a test tube. The tube is filled more or less completely with precooled water around 0 °C. Ice would normally float; therefore, we use some metal weight on top of the ice to keep the pieces at the bottom of the test tube. The ice within water reaches the lower temperature of 0 °C at the bottom of the test tube. The upper end of the test tube is then heated using a Bunsen burner until the water in the upper few centimeters of the tube starts to boil defining the upper temperature of 100 °C. The temperatures of 0 and 100 °C will be maintained as long as there is ice in the test tube (latent heat of melting) and as long as the upper parts are still covered by boiling water (latent heat of evaporation). Along the test tube, a temperature profile develops, which is mainly governed by the thermal conductivity of the water (the glass has a somewhat larger thermal conductivity). Furthermore, it is very thin such that – to first order – the Biot number can still be assumed to be small compared to unity. This means that the glass surface temperature should more or less resemble the water temperature inside the tube. Figure 5.13 depicts the experimental result from IR imaging. The line plot along the test tube shows that both glass and water are poor thermal conductors. The water at the bottom is still around 0 °C, whereas the water at the top has just boiled.

Of course, waiting for a long time will also lead to heat conduction, which will eventually equalize the temperatures.

5.3.3 Convections

In Chapter 4, convection was introduced as representing heat flow between a fluid and a solid. It is composed of both heat transfer due to conduction in the boundary layer around the solid and heat transfer due to bulk motion of the fluid that is outside the boundary layer. Both processes are difficult to visualize with IR imaging if the fluids are gases, unless the gases have strong absorption features in the thermal IR region (Chapter 7). Convections due to liquid fluids are easier to observe. Figure 5.14 depicts an ice cube, which is floating in a glass beaker filled with water at room temperature. If the ice cube and water were just at rest at the beginning, natural convection would start to build up, that is, water close to the ice cube would get cooler, thereby transferring part of its thermal energy to the cube, which would start to melt at the surface. The colder water has a higher density and will start to sink down in the beaker, thereby transporting warmer water to the surface. These slow convection currents would not be observable with IR imaging since water is not transparent in the thermal IR region (Section 1.5, Figure 1.55). However, convective bulk motion of water can be made visible by observing from above. The ice cube floats and therefore we can study the water surface convection currents. Since there is no natural lateral force driving such currents, the ice cube is given a little bit of an initial spin. Owing to this initial rotary movement some volume elements of the water, which have touched the cube and had already cooled down move, that is, flow away from the boundary layer. Therefore new water volume elements can come close to the cube transporting thermal energy from the water at room temperature to the ice cube at around freezing temperature. This leads to a melting at the ice cube surface. In Figure 5.14, water with the green shades is about 6–7 K cooler than the average water temperature. Figure 5.14 also

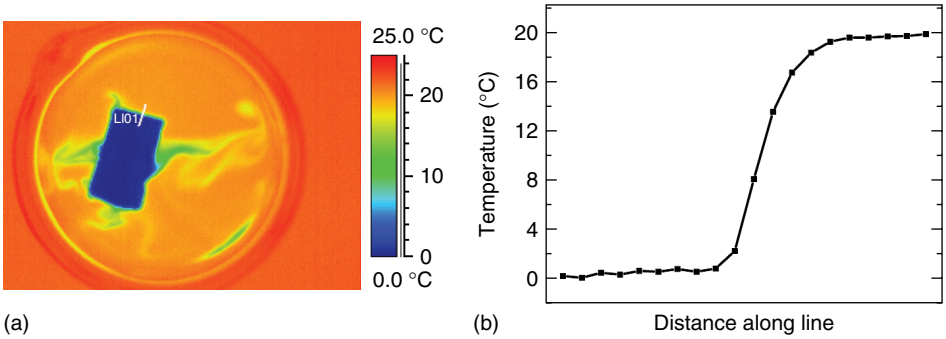

Figure 5.14 (a) Top view of water convection around a slowly rotating ice cube and (b) temperature profile along the white line. For details, see the text.

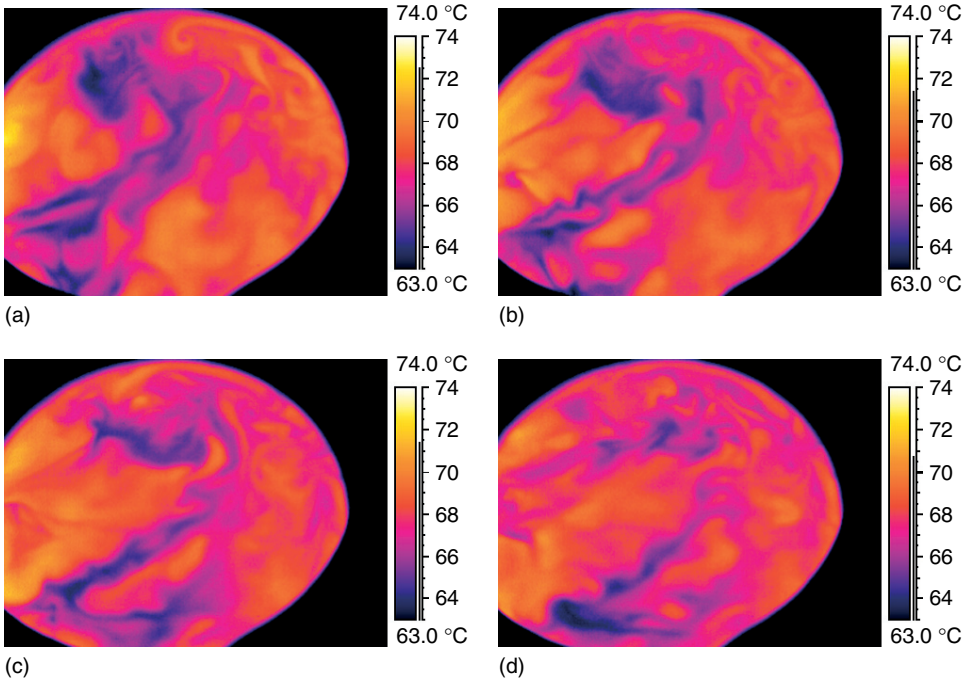

Figure 5.15 Convection features observed from a hot water surface, the water being heated from below.

demonstrates the heat conduction in the boundary layer. The line plot data in a "quiet" region show the expected gradual increase from the ice cube ($T \approx 0\ ^{\circ}$C) to the average water temperature of about 20 °C. In this case, the steep increase takes place over a distance of about 2 mm. For a nonmoving cube, the distance can easily be a factor of 2 larger. If an ice cube rests at the edge of the beaker in contact with the glass, it is also possible to directly observe cold convection currents from the outside of the beaker. This is due to cold water which starts to sink from the ice cube at the inside of the beaker thereby cooling the adjacent glass surface.

Convections with transport of larger volume elements of fluids are usually driven by larger temperature differences. A well-known example in nature is the convection cell structure, which can be observed at the surface of the sun. Figure 5.15 depicts a series of IR images, showing convection features of water within a large glass beaker being heated from below. Convection is a transient phenomenon and can be better observed in real time; however, the still images already show how structures are formed and transported across the surface of the water.

Similar convection cells are observable in everyday life when heating oil in a pan to very high temperatures. For appropriate temperature differences and oil thickness, this leads to so-called Bénard–Marangoni convections. Figure 5.16 illustrates how these convection structures form. Oil in the vicinity of the lower hot surface is heated and therefore starts to rise due to its lower density. Similarly, the

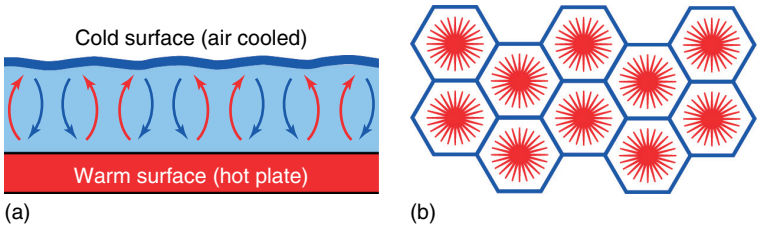

Figure 5.16 Formation of Bénard–Marangoni convections of a liquid heated from below and cooled from above. Warm oil (red) starts to rise, whereas colder oil (blue) sinks (a). This can result in (ideally) hexagonal two-dimensional structures on the surface (b), where the rising oil is in the middle of the cells and the sinking one defines the cell boundaries.

colder and denser oil from the surface starts to sink down. Of course, this process cannot take place simultaneously everywhere in the pan. For given temperature difference, oil thickness, and diameter of the pan, regular cell structures start to form, which allow large quantities of hot oil to rise while simultaneously the same amount of colder oil sinks to the bottom of the pan. In the two-dimensional sketch of Figure 5.16, closed loops of flowing oil organize in such a way that neighboring loops rotate in opposite directions such that they do not disturb the flow of their neighbors. This process is self-organizing. The form and number of formed cells depend on the conditions, in particular the temperature difference. The complete theoretical modeling needs to take into account the buoyancy forces, temperature-dependent surface tension, and dynamic viscosity of the oil [11]. Since there are regions where colder oil sinks and others where warmer oil rises, a line plot of temperature across the surface will show regular structure.

Figure 5.17 shows an example of an experimental result, investigated with IR imaging (care must be taken to avoid oil vapor on the camera optics; either a mirror can be used or a thin transparent plastic foil acting as protective window). The

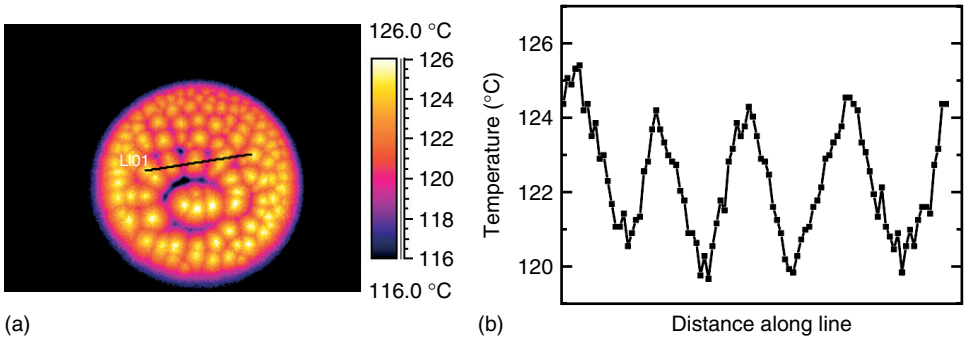

Figure 5.17 IR image of Bénard–Marangoni convection cells of oil in a pan, heated to about 120 °C (a). Convection leads to well-defined temperature variations across the surface (b).

oil thickness was 3 mm and the total diameter about 9.5 cm. The structures start to form well above 100 °C. For constant temperature the cell structure is stable; however, its geometry and number density changes with temperature. Temperature differences between rising and sinking oil amount to about 4.5 K in Figure 5.17. In a pan heated to 150 °C, we observed T variations of up to 9 K.

Some kitchen experts who want to prepare steaks in a pan use these convection cells as an indicator of the oil temperature. It is quiet easy to observe the convection cells with the naked eye when looking at grazing incidence at the oil surface. The oil is not hot enough unless the cells start to form.

5.3.4 Evaporative Cooling

The idea behind evaporative cooling can be guessed from the following description of an ancient cooling system: ''In the Arizona desert in the 1920s, people would often sleep outside on screened-in sleeping porches during the summer. On hot nights, bedsheets or blankets soaked in water would be hung inside the screens. Whirling electric fans would pull the night air through the moist cloth to cool the room'' [12]. The same article [12] by the California energy commission also emphasizes that many new technologies have been inspired by this principle of evaporative cooling.

The physics behind evaporative cooling is quite simple. One needs air with relative humidity below 100% (Section 4.3.6) which is directed over water, wet surfaces, or through wet blankets. While passing over the respective water surfaces, water molecules change their phase state from liquid to gas. Thereby the water molecules become part of the airflow, which will then have a higher humidity.

This phase change from liquid to gas does, however, require energy, to be specific, the heat of vaporization, which amounts to about 2400 kJ kg^{-1} at around 30 °C (sometimes, this number is also given as 43 kJ mol^{-1}, that is, as energy needed to vaporize 1 mol, here 18 g, of water or as 0.45 eV/molecule where one uses the fact that 1 eV = 1.6×10^{-19} J and 1 mol of water contains 6.022×10^{23} molecules). This is an enormous amount of energy that must come from either the water or the air or both. Therefore, there should be two observable effects: the water should cool down and the air should cool down. The latter effect was described above: the hot air being pulled through the wet blankets loses part of its thermal energy, which is transferred to the blankets, providing the energy for evaporation. In dynamic equilibrium, the blanket temperature would not change any more and the energy needed for the evaporation of water per time would be transferred to the blanket from the air.

Obviously, IR imaging should not try to detect air temperatures, rather, the temperature of wet surfaces that are exposed to airflow should be studied. For experiments, various liquids such as water and also aftershave lotion (which contains alcohol) were used. It is well known that a lotion containing alcohol will lead to a much more dramatic cooling effect compared to the same amount of

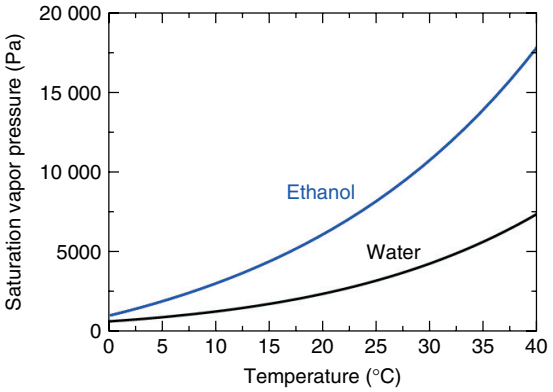

Figure 5.18 Saturation vapor pressure of ethanol and water. The differences are due to the lower boiling temperature of 78 °C, that is, the ethanol vapor pressure reaches the atmospheric pressure of about 1000 hPa already at 78 °C.

pure water. Although water and ethanol have about the same heats of vaporization (40–45 kJ mol^{-1}), they do, however, behave quite differently. This means that there is at least a second ingredient to evaporative cooling: the vapor pressure of the liquid at given ambient conditions. As shown in Figure 5.18, the saturation vapor pressure over a liquid increases steeply with temperature. The *saturation pressure* is defined as the equilibrium vapor pressure above a liquid. This means the following: some molecules evaporate per time interval from a liquid (from liquid to gas phase) and some gas molecules condense at the liquid again (from gas to liquid phase). For any given temperature, there is an equilibrium when equal amounts of molecules evaporate and condense. In this case, the gas pressure (being related to the number density of molecules in the gas phase), is the saturation vapor pressure. As shown in Figure 5.18, at any given ambient temperature between 10 and 30 °C, the ethanol vapor pressure is at least twice as large as the one of water. As a consequence, compared to evaporation of water molecules, twice as many molecules of ethanol vapor can evaporate that is, the evaporative cooling effect can be much larger.

Two more factors that have an influence on evaporative cooling are the relative humidity of the air and the speed of the airflow. If the air is already saturated with water vapor, it cannot accommodate more water. In this case, evaporative cooling cannot take place. The speed of the airflow can enhance evaporation quite appreciably. This is plausible since air in close contact with water will get higher values of relative humidity and hence it can accommodate less water vapor. Blowing fresh air of lower relative humidity toward the water surface will therefore enhance the evaporation. In addition, as was pointed out in Chapter 4 (Figure 4.4), the convective heat transfer coefficient increases with increasing airflow velocity. Therefore, larger amounts of energy for the vaporization of water vapor are available.

Figure 5.19a,b depicts an example with a water film on the wall surface of a model house. A warm air fan was directed onto the wall and the IR images were

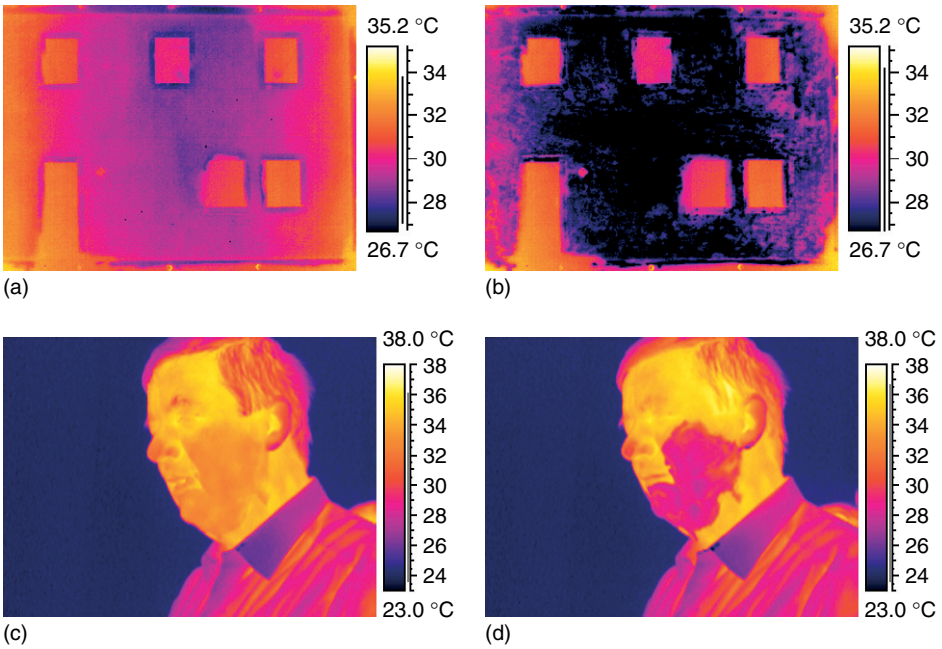

Figure 5.19 (a,b) Evaporative cooling due to water. A wet surface of a model house cools rapidly due to evaporative cooling, enhanced by a warm air fan (for details, see Section 6.4). (c,d) Evaporative cooling due to ethanol in aftershave, enhanced by a warm air fan.

recorded. Owing to evaporative cooling, the wet wall segment was strongly cooled initially, although warm air was used. Later on, after equilibrium was established, the wall temperature remained constant. Consequences for building thermography are discussed in Chapter 6.

Similarly, Figure 5.19c,d depicts evaporative cooling after using aftershave. The ethanol rapidly evaporates in particular if an airstream from a fan is used and gives rise to enhanced cooling.

5.3.5 Adiabatic Heating and Cooling

The state of any gas is usually characterized by three quantities. The most commonly used quantities are pressure, temperature, and volume; others include, for example, entropy. There are many ways of changing the state of a gas, for example, one may keep one of these quantities constant and change the other two. Two processes that are very important for technical applications are the so-called adiabatic expansions or compressions, the characteristic features of which are due to energy conservation.

Whenever a gas is compressed, work is done on the gas, which will lead to a change of its internal energy (which microscopically can be regarded as energies of the gas molecules). The first law of thermodynamics is a statement of energy conservation. It states that the internal energy of a gas can only change due to either heat transfer to/from the gas or work done on/by the gas. In most state changes of a gas, heat as well as work is exchanged. However, adiabatic processes are different. They take place too fast for thermal equilibrium to be established, and therefore adiabatic processes take place without exchange of heat. As an example, we consider a very fast compression of a gas. Assume that a gas is in a container with a movable piston. A typical everyday life example would be a pump for the bicycle tire with closed outlet valve. If the piston is moved inward very rapidly (in order to compress the gas), there is no time for exchange of heat, that is, the compression takes place as an adiabatic process. In such a case, the work done during compression is entirely transferred into internal energy of the gas. As a consequence, it will heat up rapidly. Those who use a bicycle hand pump know that the pump close to the valve gets warm quickly since the hot gas inside will finally also lead to a warming of the containing metal or plastic tube.

We illustrate the reverse process, the adiabatic expansion of a gas, with IR imaging. Expansion of a gas requires that work must be done (imagine the gas moves a piston outward upon expansion). Since heat exchange is not possible, the energy needed for this work must come from the gas itself, that is, the gas must reduce its internal energy. This goes along with a temperature decrease. This means that any adiabatic expansion will result in a decrease of gas temperature. Such adiabatic processes may be realized simply by using the tire of a bicycle, which is pressurized to 3 bar. Opening the valve leads to a rapid expansion through the valve. Therefore, the gas needs to cool down. The cold airstream touches the valve and therefore leads to a cooling of the valve. This is illustrated in Figure 5.20.

Holding a piece of paper originally at 23 °C (ambient temperature) in front of the expanding airstream leads to a rapid cooling of the paper to about 7 °C, which

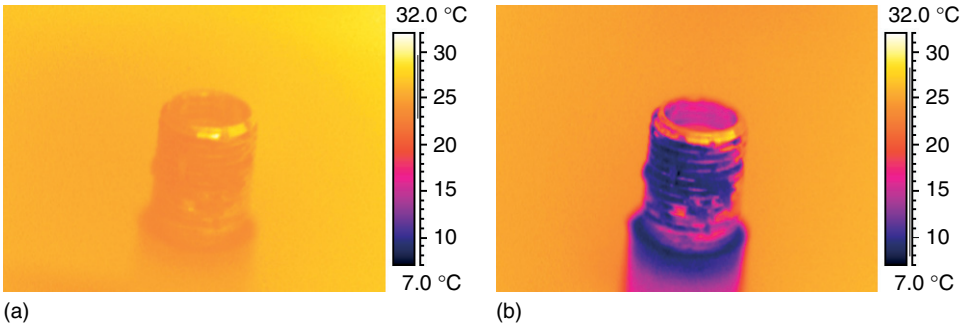

Figure 5.20 Valve of an automobile tire before (a) and after (b) opening the valve. Adiabatic cooling of expanding air from a bicycle tire leads also to a cooling of the valve with a large temperature drop.

is below its dew point at 50% relative humidity, that is, the paper gets wet during the cooling process.

5.3.6 Heating of Cheese Cubes

Several examples for heating and cooling of objects like metal cubes and light bulbs have been presented in Sections 4.4 and 4.5. In this Section and Section 5.3.7 we give additional examples related to heating and cooling of selected objects. Some of these examples illustrate the general physical principles of convection and radiation very effectively. In all cases, we assume small Biot numbers, that is, that the surface temperatures resemble something close to the average temperatures of the objects.

The first example [13] deals with cheese cubes. Imagine a piece of solid cheese, such as Gouda or Cheddar, that has no air holes in it. Cut the cheese into several, say 6–8, small cubes of sizes from 2 to 15 mm. Place the cubes in a circle on a small plate (Figure 5.21) and put the plate inside a conventional electric oven that has been preheated to 200 °C.

Question: What will happen to the cheese cubes? Will the small ones melt first or the large ones, or will all cubes melt at the same time or will some not melt at all? (The answer to this and the following question is given on the next page, to offer the possibility of thinking before reading the solution.)

After having dealt with this introductory problem, repeat the experiment, that is, prepare an identical set of cheese cubes on an identical plate, which, however, should be microwave proof. Then place the plate inside a microwave oven, which has been set at full power (e.g., 800 W). The heating should take place for an integer number of revolutions of the turntable; this ensures that all cubes experience the same microwave fields within the oven. The question will be the same as before: What will happen to the cheese cubes? Will the small ones melt first or the large ones or will all cubes melt at the same time or will there be some cubes not melting at all?

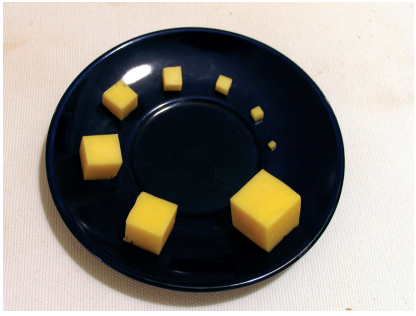

Figure 5.21 Cheese cubes of different sizes on a plate, which may be put into a conventional oven or a microwave oven.

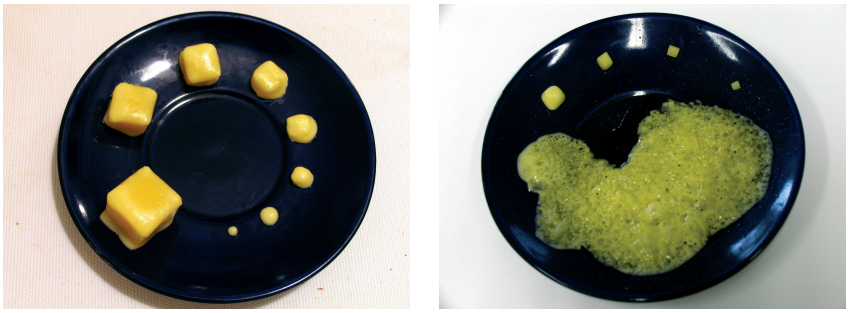

(a) (b)

Figure 5.22 In the conventional preheated electric oven, (a) the cubes were heated at 200 °C for about 70 s. The microwave oven (b) was operated at 800 W for about 30 s (for details see text).

Figure 5.22 shows the results of the cheese cube experiments heated in a conventional oven (a) and microwave oven (b). In the conventional oven the small cubes will start to melt first, which can be seen nicely by the rounding off of the corners. In contrast, the cubes behave totally differently in a microwave oven. The largest cubes melt first and it can even be observed that cubes with sizes below a critical size will not melt at all. Obviously, the different behavior must be due to the different heating and cooling processes involved.

The temperature of the air within the conventional oven is much larger than the cheese temperature. Therefore energy flows from the oven through the surface of the cubes into the cheese. The smaller cubes get heated throughout their interior much faster than the large ones and, hence, melt first. In contrast, heating in the microwave oven is realized via absorption of microwave radiation within the interior of the cheese cubes [14]. However, since the air temperature within the oven is about ambient temperature, the heated cheese cubes also start to cool via convection and radiation. The cooling power will be proportional to the surface area of the cubes, whereas the heating will be proportional to their volume. As a consequence, the surface-to-volume ratio determines a final maximum temperature of a cube. The smallest cubes will suffer the most effective cooling. Eventually, this can even prohibit melting. The final temperature will increase with cube size. This is shown in Figure 5.23, which depicts the situation after 10 s of heating. The quantitative analysis revealed a strong dependence of temperature on cube size and the temperatures of the largest cubes were above melting temperatures of the cheese.

The heating and cooling of cheese cubes in the microwave oven can also be easily treated theoretically [13]. The power absorbed by each cheese cube of size a is proportional to its volume:

$$\frac{dW_{\text{abs}}}{dt} = P_{\text{absorb}} \propto V = k_1 a^3 \tag{5.1}$$

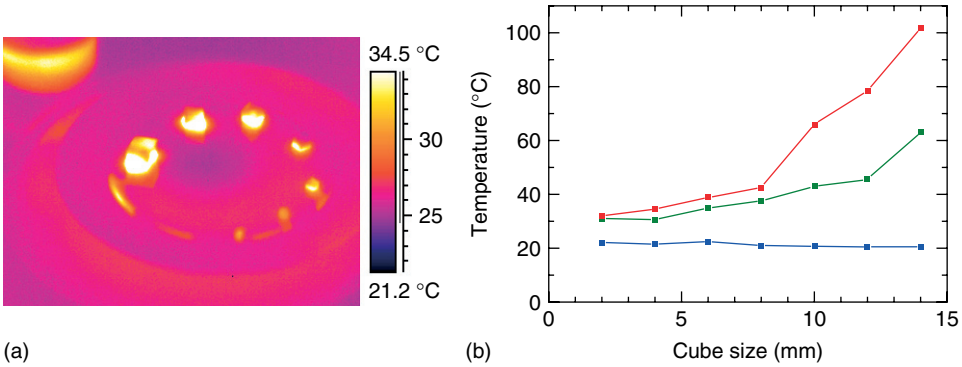

Figure 5.23 Cheese cubes after 10 s of heating (800 W) within a microwave oven (a) and measured maximum temperatures of the cubes before (blue, bottom), after 10 s (green, middle), and after 30 s (red, top) of heating (b).

where k_1 is a constant which depends on the absorption coefficient of microwaves in cheese. The cooling, which is due to convection and radiation (Section 4.2) can be approximated by

$$P_{\text{cool}} = k_2 \cdot a^2 \cdot (T_{\text{cheese}} - T_{\text{oven}}) \tag{5.2}$$

It depends linearly on the temperature difference between the cheese and its surrounding. The effective absorbed power leading to a temperature rise of the cheese is due to

$$P_{\text{eff.heating}} = P_{\text{absorb}} - P_{\text{cool}} \tag{5.3}$$

This leads to the differential equation

$$P_{\text{eff.heating}} = c \cdot m \cdot \frac{dT}{dt} = k_1 \cdot a^3 - k_2 \cdot a^2 \cdot \big(T(t) - T_0\big) \tag{5.4}$$

with the solution

$$T(t) = T_0 + \frac{k_1}{k_2} a \left[1 - e^{-\frac{(t-t_0)}{\tau}}\right] \tag{5.5}$$

with the time constant $\tau = 1/A = k_3 a$. Despite not knowing exact values for the constants, it is possible to plot the general form of $T(t)$ as shown in Figure 5.24 for different values of cube size a. It follows from Eq. (5.5) that the temperature of each cube eventually reaches the asymptotic value $T_0 + \frac{k_1}{k_2} a$. If this temperature is below the melting temperature, the cheese will never melt. An interesting feature of Eq. (5.5) is that since the time constant τ is proportional to cube size, the time until the maximum temperature is reached at equilibrium conditions is shortest for small cubes. As shown in Figure 5.24, only the smallest cubes have reached the maximum possible temperature, whereas the largest cubes are still far away from equilibrium.

More details on this experiment can be found in [13].

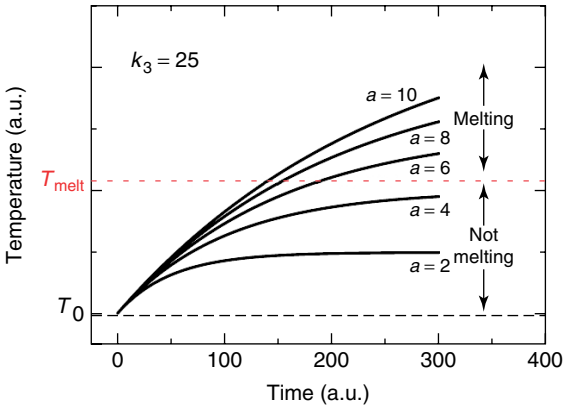

Figure 5.24 Temperatures of cheese cubes of different sizes a as a function of heating time in a microwave oven for a given value of $k_3 = 25$ (i.e., e.g., $\tau = 50$ for $a = 2$).

5.3.7 Cooling of Bottles and Cans

The second example concerns an everyday experiment using Newton's law of cooling (Section 4.5). Whenever an object of temperature T_{obj} is in a surrounding of lower temperature T_{surr}, it will cool down due to convection and radiation losses. Energy conservation requires that the heat losers lead to a decrease in thermal energy and hence in the temperature of the object. In this case, the cooling process is described by

$$mc\frac{dT}{dt} = -(\alpha_C + \alpha_R) \cdot S \cdot (T_{obj} - T_{surr}) \quad \text{where} \quad \alpha_R = \varepsilon \cdot \sigma \cdot k_{appr} \tag{5.6}$$

This differential equation has the solution

$$T_{obj}(t) = T_{surr} + (T_0 - T_{surr}) \cdot e^{-t/\tau} \quad \text{with} \quad \tau = \frac{\rho cV}{(\alpha_C + \varepsilon \cdot \sigma \cdot k_{appr})S} \tag{5.7}$$

Equation (5.7) means that if Newton's law of cooling is fulfilled, we expect an exponential decrease of the temperature difference with time, that is, a straight line in a semilogarithmic plot (Section 4.5). This expectation was checked by studying the cooling of soft drink cans and bottles. Particularly in summer time, the cooling of liquids in refrigerators is of importance. As two examples we measured the cooling of cans and bottles filled with water (or other liquids) as a function of time for different cooling methods. Figure 5.25 depicts the experimental setup.

The cooling power of the systems is expected to be quite different. The conventional fridge and the freezer both have objects surrounded by still air, since the temperatures are usually too low to generate natural convections. Hence, the heat transfer coefficients and the cooling time constants of both should be the same. However, the refrigerator has a smaller temperature difference than the freezer; therefore, the cooling power of the freezer is larger and the effective cooling times

Figure 5.25 Cooling cans and bottles of liquids in a conventional refrigerator ($T_{final} = 6\ ^{\circ}C$, not shown), a freezer ($T_{final} = -22\ ^{\circ}C$), and an air convection cooler ($T_{final} = -5.5\ ^{\circ}C$). A tape of known emissivity ($e = 0.95$) was attached to bottles and cans.

(times to reach a certain low temperature upon cooling) are smaller than in the refrigerator. The air convection cooler should have the fastest cooling since the convective heat transfer coefficient increases strongly with airflow velocity. Therefore, the time constant should also decrease.

As samples, we used glass bottles and aluminum cans. A (blue) tape was attached in order to ensure equal emissivity values for all samples. The containers were filled with water slightly above room temperature and placed inside the refrigerator, freezer, and air convection cooler. During temperature recordings with the IR camera, taken every few minutes, the cooling unit doors were opened for utmost 25 s each. Figure 5.26 shows the resulting plots of temperature difference between measured temperature and ambient temperature within the cooling system on a logarithmic scale. From Newton's law a straight line is expected. Obviously, this holds quite well for any cooling mechanism down to around 0 °C, where the phase transition water to ice imposes a natural limit. At the end of the experiments in the freezer and air convection cooler, we could indeed observe small pieces of ice, floating on the surface of the water in the bottle and the can.

The time constants τ from quantitative fits to the data nicely agree with theoretical expectations from Eq. (5.7). For the freezer and the refrigerator, $\tau \approx 8300–8400$ s, whereas for the air convection cooler, the value of τ is halved. This is due to the increased convective heat transfer coefficient. Theory also accounts for the differences (a factor in τ of about 1.2) between cans and bottles. It is, on one hand, due to the different amounts of water and, on the other hand, due to the differences in the stored thermal energy in the glass of the bottle as compared to that in the aluminum can.

The user of cold drinks is usually not interested in time constants, rather he/she would like to know at what time, a drink will reach a certain temperature. Figure 5.27 depicts the experimental cooling curves for the 0.5-l bottles

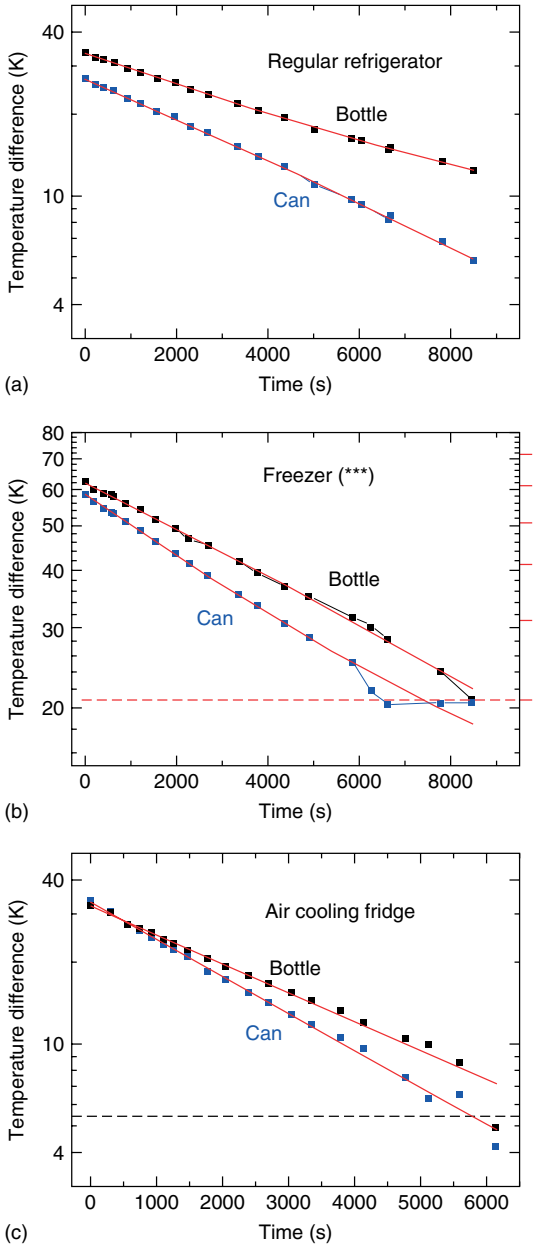

Figure 5.26 Cooling curves of can and bottles for a regular fridge, a freezer, and an air convection cooler. All plots can be fitted with a simple exponential, that is, they follow Newton's law of cooling.

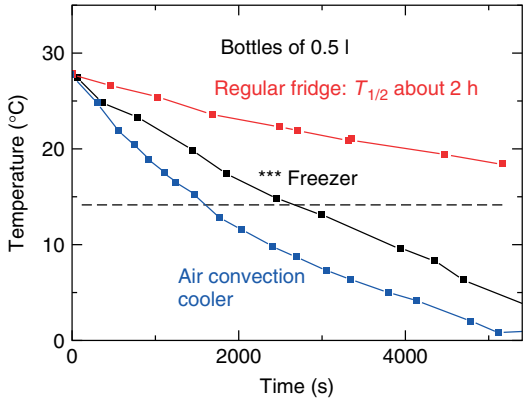

Figure 5.27 Cooling curves of 0.5-l bottles for a regular fridge, a freezer, and air convection cooler. The typical timescale for cooling from 28 °C to below 14 °C (which may be a suitable drinking temperature) is above 2 h for the fridge, about three-fourth of an hour for the freezer, but less than half an hour for the air convection cooler.

(linear scale). The initial temperature was about 28 °C. The fridge has the longest cooling time, whereas the air convection system cools fastest, for example, in about 30 min from 28 °C to below 13 °C.

Obviously, from daily experience, an even faster way of cooling would use forced convective cooling with liquids rather than gases, due to the large density difference between gas and liquid.

5.4 Electromagnetism

5.4.1 Energy and Power in Simple Electric Circuits

In any simple electric circuit that follows Ohm's law [5, 6], electrical energy is transferred into internal thermal energy within the resistor, revealing itself as a temperature rise of the resistor. Obviously, IR imaging can easily visualize this direct thermal consequence of electric currents through resistors. Figure 5.28 depicts the simplest electrical circuit: a wire is connected to a power supply. The wire itself is the resistor, which warms up while current is flowing through the wire.

Figures like 5.28 can also visualize that the heating of the wire before and after a coil is the same. This may help to get rid of misconceptions of students, that the current may have lost part of its "power" while traveling through the circuit, leading to less energy dissipation behind a coil.

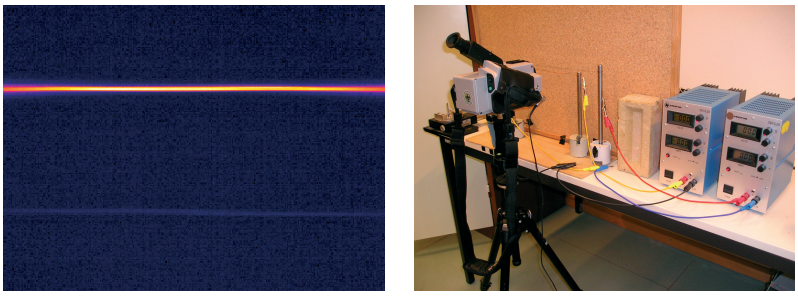

(a) (b)

Figure 5.28 The electrical energy associated with a current flowing through a wire is dissipated, leading to a temperature rise of the resistor, that is, the wire. The wire need not be straight. It can also be a coil or a wire spiral as in light bulbs. In the image, two Cu wires of different diameters (0.25 and 0.55 mm) were used with the same current of 0.5 A. As expected, the thin wire became very hot, whereas the thick wire only warmed up a little bit.

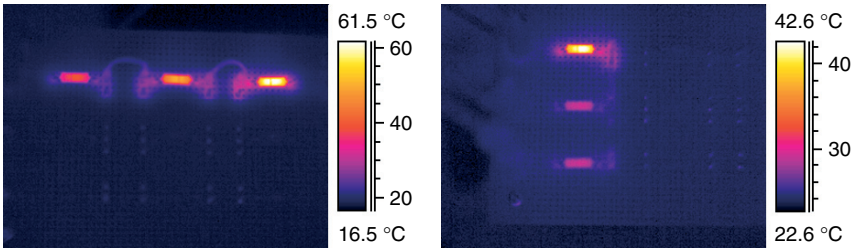

(a) (b)

Figure 5.29 Three different resistances (a) in series and (b) in parallel.

Usually, in electrical circuits, the electrical energy is not just dissipated in heating the metal wires, which are the connecting elements in the circuit. It is straightforward to design simple circuits with wires and resistors of varying size. Figure 5.29 depicts series and parallel circuits of several resistors. Obviously, the resistors heat up according to the power $P = R \cdot I^2$ dissipated within them. Measurement of the surface temperatures of these resistors then allows to sort them according to their size. Quantitative analysis, that is, to find the exact value of R from the surface temperature is a more complex problem. In this case, all heat transfer modes, conduction, convection, and radiation must be treated. In any case, studying various combinations of resistors with IR imaging may be a nice visualization of Kirchhoff's rules in simple electric circuits.

5.4.2 Eddy Currents

Faradays law of induction [5, 6] leads to a phenomenon called *eddy current*. Whenever a conducting material in the form of a loop is exposed to a changing magnetic field, Faradays law states that an electromotive force is induced. In a closed loop, this leads

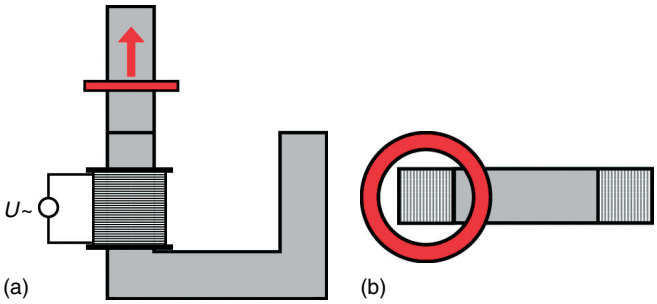

Figure 5.30 Setup for jumping ring experiment (a) from side and (b) from top. A conducting nonmagnetic metal ring (red) is placed over the extended vertical core of a demountable transformer.

to a ring current. Any current in a conductor dissipates energy according to $P = I^2 R$, that is, the current should heat up the object. The same happens if conductors of arbitrary geometrical form are exposed to changing magnetic fields. In any case, electromotive forces are induced, which lead to closed loop currents within the conductor, raising the temperature of the conductor. These currents are called *eddy currents*. These circulating currents by themselves create induced magnetic fields that oppose the change of the original magnetic field due to Lenz's law.

The effect of eddy currents can be made visible using IR imaging. Figure 5.30 depicts the setup for a popular physics demonstration, the jumping ring experiment [15, 16]. A nonmagnetic metal ring is placed on top of a solenoid over the core of a U-shaped demountable transformer unit. When AC power is applied to the solenoid, the ring is thrown off since the induced eddy currents induce secondary magnetic fields that are opposed to the primary magnetic field.

The heat generated by the eddy currents can be made visible by preventing the ring from being thrown off. Holding it by hand is not very wise; we arranged for a metal bar several centimeters above the solenoid to serve as a mechanical stop. Applying an AC power to the solenoid throws the ring to the stop, where it levitates for the rest of the experiment. Owing to the AC magnetic fields, eddy currents are permanently induced, that is, there is a continuous generation of heat according to $P = I^2 \cdot R$, which leads to a rapid heating up of the ring. Figure 5.31 depicts an example as observed after several seconds. One may study the heating as a function of time as well as differences due to different ring materials (e.g., copper vs aluminum).

5.4.3 Thermoelectric Effects

There are a number of thermoelectric effects [17] that are exploited in physics and technology. Temperature measurements with thermocouples use the Seebeck effect (Figure 5.32a).

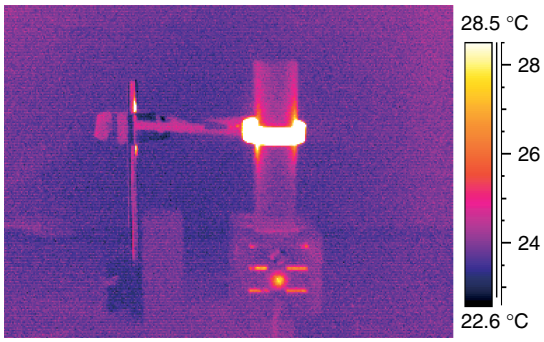

Figure 5.31 Eddy currents induced in a metal ring by the AC magnetic field in the solenoid of the open transformer unit lead to a temperature rise of the ring.

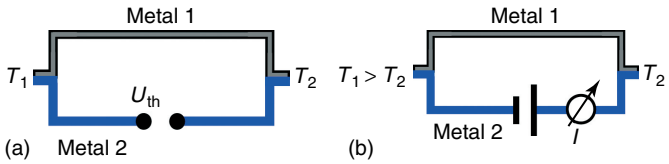

Figure 5.32 The thermoelectric Seebeck (a) and Peltier effects (b), (for details see the text).

Two different metals are joined at two points. If a temperature difference occurs between these two contact points, a small electric voltage U_{th} (typically, in the microvolts per Kelvin range) is produced, which drives a thermoelectric current. The physics behind the effect is as follows: for each metal, there exists a well-defined work function, which describes the minimum energy needed to remove an electron from the metal surface. If two different metals with differing values of their work function touch each other, there will be an electron transport from the metal with the lower work function to the one with the higher work function. This leads to a contact potential. If two metals are bent such that they touch each other at two ends, the same contact potentials will result, that is, they will cancel each other. However, the number of electrons transferred from one metal to the other depends on the temperature of the contact point. Therefore, a temperature difference between the two contact spots of two metals in Figure 5.32 will lead to a net potential difference U_{th} which depends on temperature. After calibration, this voltage is used for a quantitative measurement of temperature. In conclusion, the Seebeck effect creates a potential difference (i.e., a voltage) from a temperature difference.

The opposite effect, called *Peltier effect* (Figure 5.32b) uses an electric current to generate a temperature difference. In this case, an electric current is driven through a bimetallic circuit that is maintained at uniform temperature. Heat is generated at one junction, leading to an increase in temperature, and heat is extracted at the other junction, leading to a cooling of the junction. The direction of the current and the contact potentials determine which contact point is heated and which is

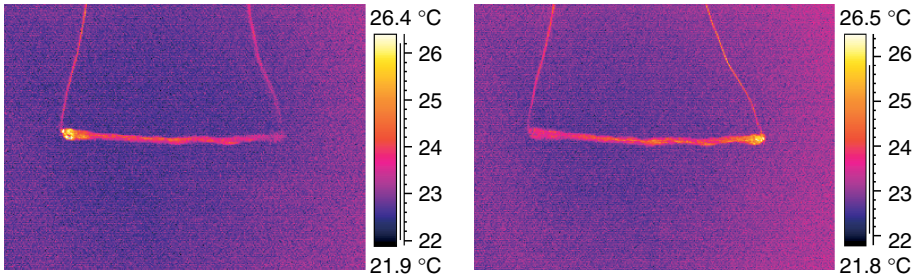

Figure 5.33 Demonstration of the Peltier effect with wires of two different materials (vertical wires, copper; horizontal wire, constantan), which produce a thermoelectric force of 42.5 $\mu V\,K^{-1}$ in the temperature range from −200 to 500 °C.

cooled. Figure 5.33 depicts an example using two copper wires (vertical) and one constantan wire. A direct current of 3 A leads to heating of one connection and cooling of the other. The effect is reversed if the direction of the current is reversed.

In this (macroscopic) experiment, the constantan wire was made much thicker (several parallel wires) since it has a higher resistance compared to the copper wire. If a single wire were used, the dissipation of energy by its resistance alone (the I^2R joule heat) would lead to a homogeneous heating along the wire, which would cover up the small effect due to the Peltier effect. Nowadays, the Peltier effect is widely used in microscopic setups of cooling systems for microelectronics and detectors (Section 8.4.2).

5.4.4 Experiments with Microwave Ovens

Microwave ovens, which are also part of everyday life, combine electromagnetism, the general behavior of electromagnetic waves, and thermal physics in a unique way. The most common application is just heating of food, but industrial ovens are also used to dry a variety of goods [18, 19]. Here, some experiments with household microwave ovens are presented (for more information, see [14, 20–22]).

5.4.4.1 Setup

Figure 5.34 depicts the main features of a microwave oven. The microwaves are generated within a magnetron and guided into the cooking chamber, which has metal walls. There, the microwave energy is absorbed [14, 18] by the food or the object placed into this chamber.

To first order, a microwave oven with metallic walls resembles a three-dimensional resonator for electromagnetic waves. The microwaves of typical ovens have frequencies of about 2.45 GHz, giving wavelengths of about 12.2 cm. The problem is solved from the equations of electrodynamics for a chamber with lengths L_x, L_y, and L_z (typical lengths range between 20 and 30 cm, i.e., 8–12 in.).

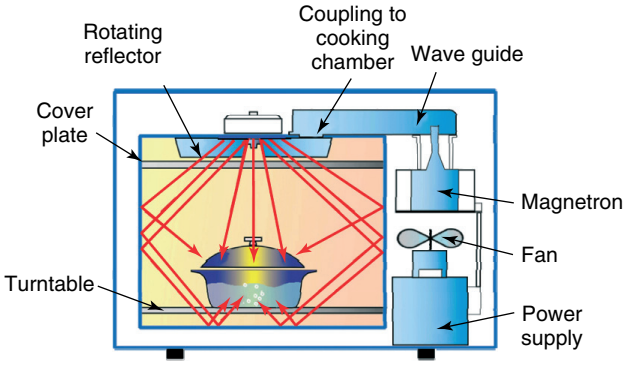

Figure 5.34 Schematic diagram of a microwave oven.

Similar to the one-dimensional case of standing waves on the string of a guitar, one finds three-dimensional standing waves, that is, there will be positions within the oven where there is a high energy density of the microwave field and there will be nodes of the standing waves, where there will be no energy density. In this respect, one speaks of horizontal and vertical modes of the microwave field.

An obvious consequence of nonhomogeneities of the microwave energy within the oven is that the absorption of the microwave energy by food or other products will strongly depend on the position. In order to reduce uneven heating of food, the effect of the horizontal modes is usually smeared out by using a rotating turntable and sometimes a top rotating reflector.

5.4.4.2 Visualization of Horizontal Modes

In order to visualize the undisturbed mode structure within a microwave oven (i.e., without turntable) using thermography, we place a thin glass plate of appropriate dimensions within the oven. Its height can be adjusted by placing Styrofoam below it. The glass does not absorb microwaves strongly. In order to measure the mode structure, we either put a wet paper on top of the plate or wet the glass plate by covering it with a thin film of water. The plate is then heated in the oven for a certain period (depending on the applied power). Directly after the heating, the door is opened and the plate is analyzed with the IR camera. Figure 5.35 depicts three examples of the observed mode structure of the otherwise empty microwave oven for the plate at the floor, in a height of 3.5 and 8 cm. In all cases, the oven was operating for 15 s at a power reading of 800 W. One clearly observes pronounced differences, that is, the horizontal mode structure also strongly depends on height.

Unfortunately, the situation is more complex for practical applications. Most importantly, the mode structure changes upon filling the oven. For example, when an object of given geometry, which can absorb microwave energy, is placed in the oven, the electrodynamic calculation of the loaded oven gives different mode structures compared to the empty oven, since the boundary conditions have changed.

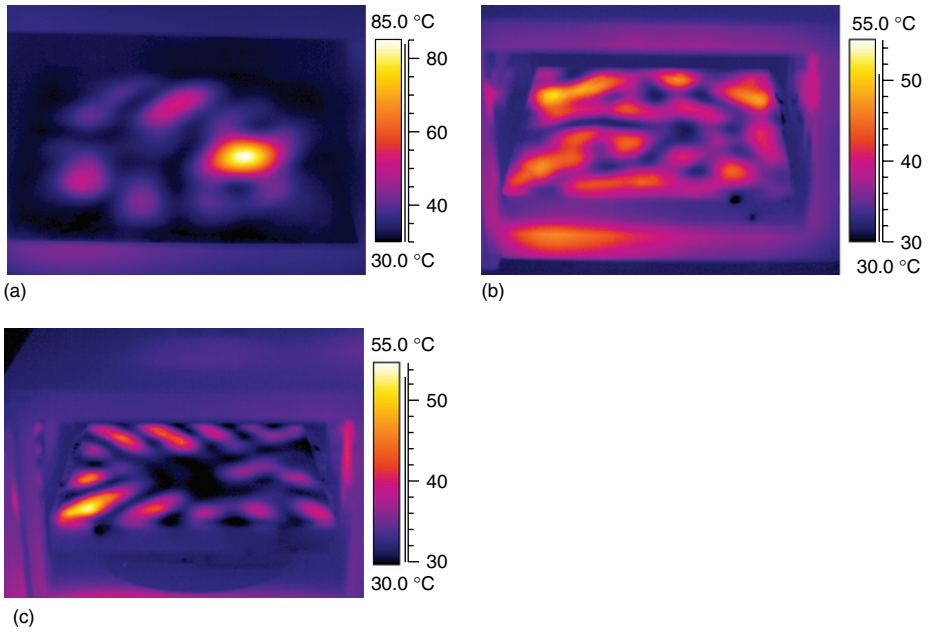

Figure 5.35 Visualization of the horizontal mode structure in a microwave oven. A glass plate with a thin water film was placed at the floor and heated for 15 s with a microwave power of 800 W without using the turntable. The plate was at the floor (a), at a height of 3.5 cm (b), and at a height of 8 cm (c).

5.4.4.3 **Visualization of Vertical Modes**

Although a turntable in a microwave oven may be useful in smearing out nonhomogeneities of the horizontal mode structure, it does not have the same effect for the vertical modes. Figure 5.36 shows IR images of a tall glass cylinder of about 2-cm diameter filled with water before and after heating in the microwave oven. The cylinder was placed in the center of the turntable, which is what most people do with objects when placing them into a microwave oven. Obviously, the heating is quite uneven. There are large temperature differences of more than 20 K between the bottom, middle, and top of the glass. In this case, we found the temperatures to be 76 °C at the top, 43 °C in the middle, and 62 °C at the bottom of the glass. If baby food is heated in this way, and the cold part is on top, one may erroneously assume that the whole food is cold enough to eat. We conclude that all food in tall containers should be stirred before serving. Of course, the turntable may help partially, but only if the container is not placed at the center, since – at fixed height – the object may eventually also move through maxima as well as minima of the mode structure, which may lead to some averaging.

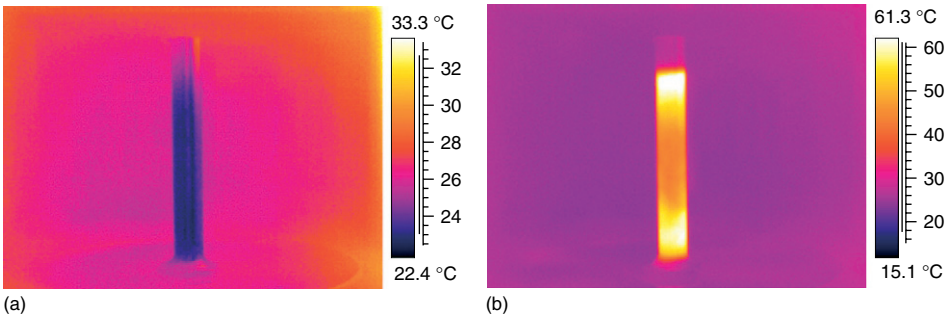

Figure 5.36 Visualization of the vertical mode structure in a microwave oven. A glass cylinder (diameter 2 cm), filled with about 30 ml of water was placed on the turntable and observed before (a) and after (b) heating for 15 s with a microwave power of 800 W.

5.4.4.4 Aluminum Foil in Microwave Oven

One often hears the statement that metals or objects with metallic parts should never be put into the microwave. Physicists know about the origin of this "wisdom;" however, also they are also aware of the limited range of validity. When microwaves interact with metals, they are not only effectively absorbed but also reradiate most of the energy. Since metals have a good thermal conductivity the fraction of the energy that is absorbed is rapidly distributed over the whole metallic body. If this body is very massive – as, for example, the walls of the microwave oven – the new equilibrium state, which depends on absorbed power, heat capacity, and heat losses corresponds to a very small warming. The behavior of smaller metal parts depends, however, strongly on their geometry and mass. Very thin metal sheets or similar bodies have only a very small heat capacity and can warm up quickly. This can even lead to glowing and evaporation, for example, from plates with golden edges. One should never put such plates in a microwave, unless the golden edge should be removed.

This leads to the typical question of what happens to thin metal foils like aluminum foil in a microwave oven. Thin strips of foil can heat up quickly, but what happens, if they have good thermal contact with another body that may absorb energy? Figure 5.37 shows two identical beakers filled with water before (a) and after (b) heating in the microwave oven. The right beaker in each image is surrounded by aluminum foil of about 30-µm thickness. This foil is thick enough such that no microwave radiation may penetrate through it, that is, in this beaker, only radiation from the top may reach the water. The foil does absorb a little bit of energy which is transferred to the water inside the beaker due to the good thermal contact. However, this energy transfer is much smaller than the energy that is absorbed in the other beaker by the water itself. Therefore, the beaker filled with water heats up much more quickly. Consequently, food should never be put in the microwave oven if it is surrounded by thick aluminum foil.

There are many more experiments that can be done with IR imaging and microwave ovens [14, 20–22].

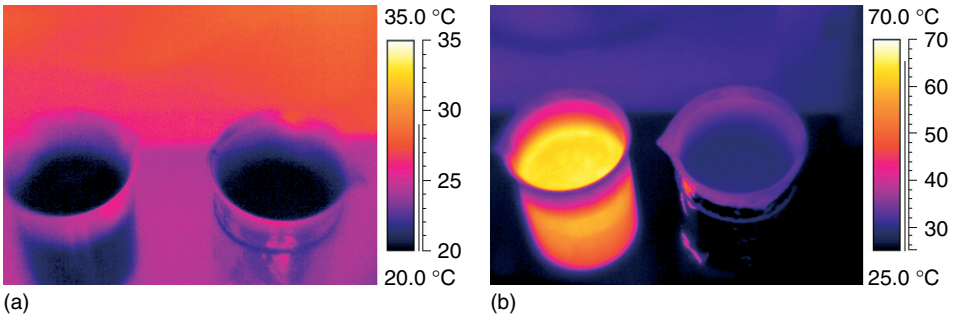

Figure 5.37 Two beakers are filled with water. The one wrapped in aluminum foil heats more slowly than the one without foil.

5.5 Optics and Radiation Physics

IR imaging can provide some fascinating insights into the optical properties of various materials and objects. Some objects are transparent in the Vis range, but opaque in the thermal IR and vice versa, and others are transparent in both spectral ranges. The general theoretical background has been discussed in Section 1.5; some simple experimental results are presented here. Infrared thermal imaging is based upon the laws of radiation by Kirchhoff and on Planck's law, describing the spectrum of thermal radiation. It also depends on emissivity and the fact whether gray or selective emitters are studied. Besides using these laws, one may, however, also use IR imaging to visualize these concepts.

5.5.1 Transmission of Window Glass, NaCl, and Silicon Wafer

Regular window glass or laboratory glass like BK7 show no transmission above $\lambda \approx 3\ \mu m$ (Figure 1.54). Therefore, any IR camera operating at longer wavelengths (LW cameras) will not be able to look through thick layers of glass, MW cameras may still see a tiny bit of radiation (See also Figure 3.2). This is known to thermographers doing outdoor building inspections; however, sometimes special care has to be taken since inhabitants of the houses can get the feeling that someone is observing them and even taking pictures through the window.

Figure 5.38 depicts someone holding a plate of glass (thickness of several millimeters) partially in front of his face. Obviously, it is not possible to look through glass, which is opaque in the IR spectral range. One may, of course measure the surface temperature of the glass plate, something which is regularly done in building inspections. In addition, Figure 5.38 visualizes one of the major problems encountered in thermography of flat surfaces; they may lead to thermal reflections, which can give rise to problems in quantitative analysis (Section 9.2).

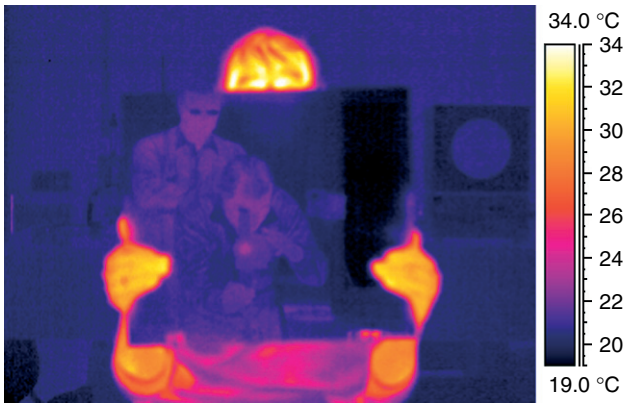

Figure 5.38 A room temperature glass plate is opaque to IR radiation. In addition, due to the flat surface, it serves as a source of thermal reflections, here two people standing behind the IR camera.

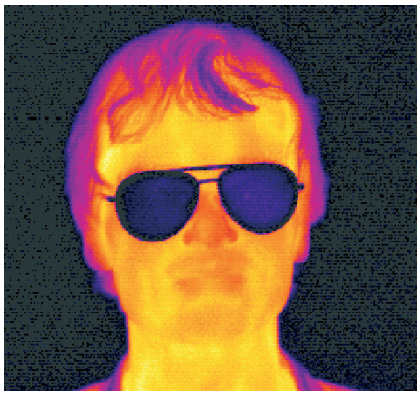

Figure 5.39 IR images of people, wearing glasses often suggest that dark sunglasses were used.

Objects made of glass are very often encountered in IR imaging, not only in building inspections but also when taking images of people. Everyone wearing regular glasses will appear in IR images as wearing very dark sunglasses (Figure 5.39) since the glass is opaque. But why is the glass temperature so much lower than the skin temperature? Glasses usually only have poor thermal contact with the face, and little thermal energy is conducted from the skin to the glasses at the three contact points at the nose and near the ears. Therefore, the heat transfer via convection from the ambient temperature air at the glass surfaces dominates and determines the surface temperature.

Figure 5.40 depicts Vis and IR images of a person using another pair of glasses. One lens is made of regular glass, the other of NaCl. From Figure 1.48, it is obvious that NaCl will transmit Vis and thermal IR radiation; therefore, one can readily look

(a) (b)

Figure 5.40 A special pair of glasses, made of two different materials; visible radiation is transmitted by both materials, whereas thermal IR radiation is only transmitted by one of them.

through the lens and observe the higher temperature of the skin near the eye. It is easily possible to use the known theoretical transmission of NaCl (about 91%) and therefrom calculate correction factors for quantitatively measuring temperatures behind the lens [23].

In contrast to glass and NaCl which are both transmitting visible radiation, silicon wafers are opaque in the Vis spectral range (spectrum Figure 1.51). Therefore, it is not surprising that one cannot look through with the eye. IR imaging does, however, allow looking through matter (Figure 5.41).

In the experiment, a wafer of 0.362 mm thickness was placed directly in front of the IR camera lens. The real part of its index of refraction (3.42) leads to a transmission of about 53%.

5.5.2 From Specular to Diffuse Reflection

Usually, only the law of mirror reflection (here denoted as specular reflection) is treated (Eq. (1.2), Figure 1.9), when introducing reflection in optics. In contrast, diffuse reflection is encountered much more often in everyday life and technology, or at least a combination of diffuse and regular reflection, as illustrated in Figure 5.42.

The transition from pure specular reflection (e.g., from a mirror) to pure diffuse scattering (e.g., from a wall or blackboard) can be nicely studied using IR imaging with LW cameras. Diffuse scattering takes place if the wavelength of the electromagnetic radiation is comparable to the dimensions of the surface roughness. If the latter dimensions are small compared to the wavelength, regular reflection takes place. Analogously, a soccer ball will bounce back from a mesh wire according to the law of reflection, whereas a table tennis ball with similar dimension than the mesh will behave like a diffuse scatterer.

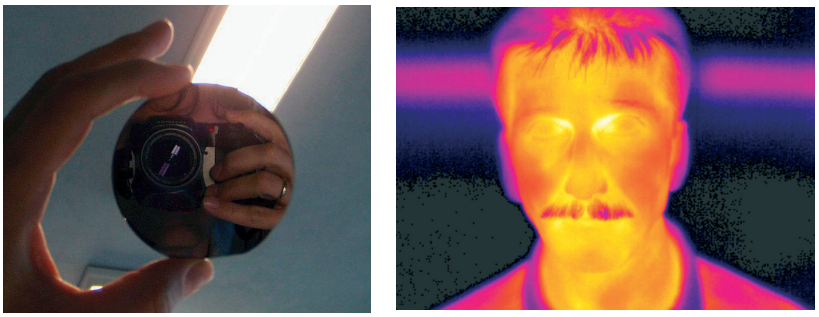

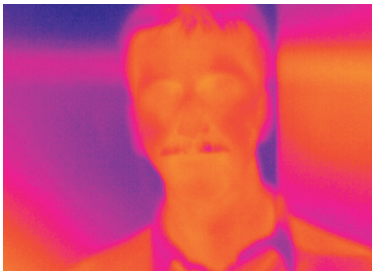

Figure 5.41 A Si wafer – polished on both sides – is opaque for visible light (a), but transmits thermal IR radiation (c). The IR signal is just attenuated according to the Si transmission compared to the image without wafer (b)

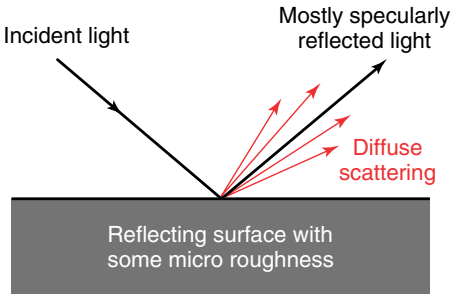

Figure 5.42 Real surfaces have surface roughness. Therefore, reflection consists of a superposition of specularly reflected and diffusely scattered light.

Using visible and IR electromagnetic radiation the transition from diffuse to specular reflection can be demonstrated directly. Consider, for example, a person in front of a brass plate which is oxidized and a diffuse scatterer in the visible ($\lambda = 0.4-0.8\,\mu m$): no mirror image can be seen (Figure 5.43). However, the wavelength of the IR radiation, detected in $\lambda = 8-14$-μm IR cameras is about a

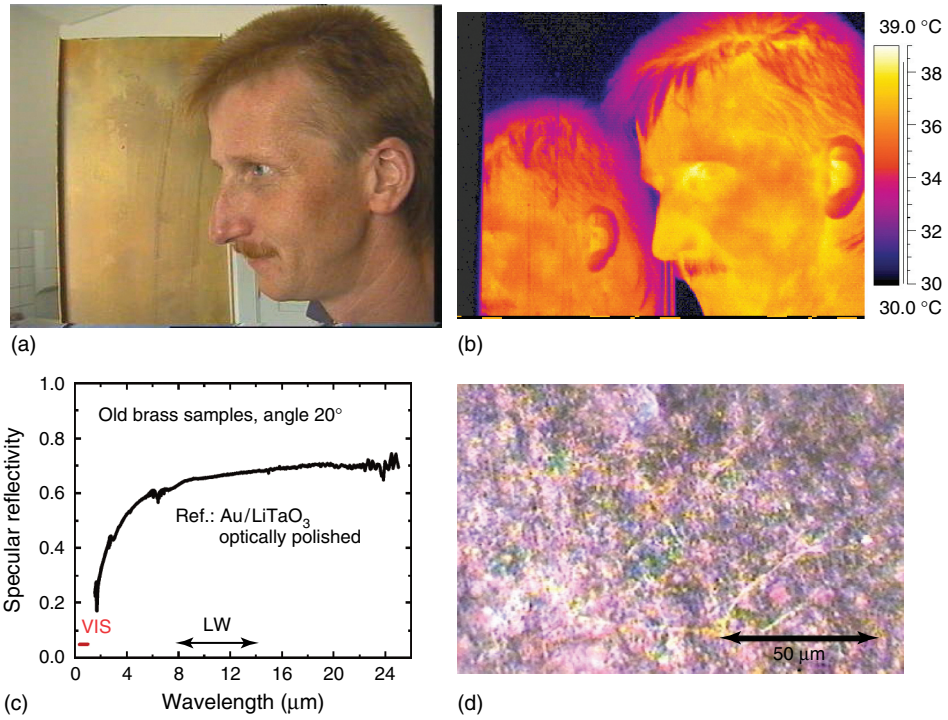

Figure 5.43 (a) Transition from specular to diffuse reflection, an oxidized brass plate scatters visible light diffusely, whereas LW IR radiation leads to a clearly observable specular reflection image. (b) This behavior is due to microscopic roughness (see electron microscope image (d)), which also shows up in the specular reflectance spectrum (c).

factor of 10 larger. Therefore, the IR image can demonstrate regular reflection (for more details, see Section 9.2 and [24]).

5.5.3 Blackbody Cavities

Blackbody cavities (Section 1.4.6) are considered to give the best possible approximations to blackbody radiation on earth. Therefore, many theoretical analyses were done on theoretical emissivities depending on properties of the used cavities. According to an old theory by Gouffé, the total emissivity of a cavity resembling a blackbody is given by [25]

$$\varepsilon = \varepsilon_0'(1 + \gamma) \tag{5.8}$$

where

$$\varepsilon_0' = \frac{\varepsilon^*}{\varepsilon^*\left(1 - \frac{s}{S}\right) + \frac{s}{S}} \tag{5.9a}$$

and

$$\gamma = (1 - \varepsilon^*)\left[\left(\frac{s}{S} - \frac{s}{S_0}\right)\right] \tag{5.9b}$$

In these equations, ε^* denotes the emissivity of the wall material of the cavity, s and S are the areas of the aperture and of the interior surface, and S_0 denotes the surface area of an equivalent sphere, which would have the same depth as the cavity in the direction normal to the aperture. Usually γ is a small number; however, depending on the cavity shape it can be positive or negative.

From Eqs. (5.8) and (5.9) it becomes clear that even quite small numbers of material emissivity can give quite large values for the total emissivity.

Figure 5.44 shows the results of an experiment. A set of three cylindrical holes in a metal block could be covered by apertures to form cavities of different emissivities. IR images of the heated cavities revealed that the apparent temperature between the largest and the smallest aperture cavity evaluated for constant emissivity would

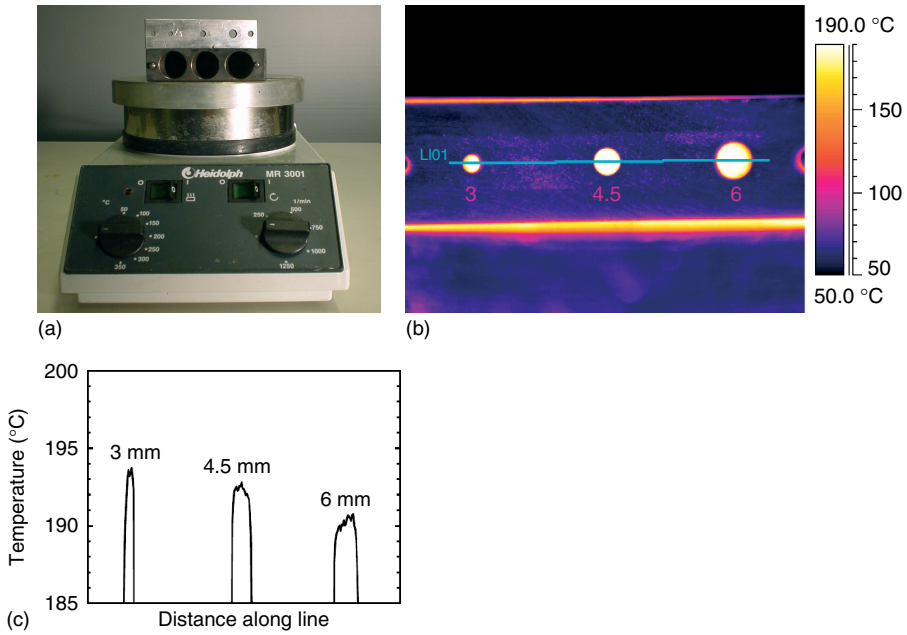

Figure 5.44 (a) A set of three cylindrical holes in a metal block, which may be covered by apertures of different sizes to form cavities of different emissivities. (b) IR radiation was detected when heating the cavities to a temperature around 200 °C. (c) The temperature along a line through the centers of the holes was evaluated for constant emissivity (for more details see the text).

differ by more than 2 K. Assuming, however, that the differences in detected IR radiation are due to changes in emissivity, the experiment nicely demonstrates the validity of Eqs. (5.8) and (5.9).

The cylindrical holes had an inner diameter of 18 mm and a depth of 36 mm each. The apertures used had diameters of 3, 4.5, and 6 mm, leading to values $(s/S) = 0.28$, 0.62, and 1.1% respectively. The values of (s/S_0) are even smaller; hence the correction term γ is always below 0.01. The metal walls of the cavity were already slightly corroded and had $\varepsilon^* \approx 0.21$. This gives total emissivities of the three cavities of about 0.96 for the 6-mm aperture, 0.98 for the 4.5-mm aperture, and 0.99 for the smallest 3-mm aperture. These small differences in emissivity directly and quantitatively explain the observed results from the IR analysis (Figure 5.44).

We note that the front plate looks much colder than the holes in the IR image. This is due to the lower emissivity of the cover plate (see visible image). Repeating this experiment for a long time leads to oxidation of the front surfaces, which goes along with an increase in emissivity. Therefore, the actual IR image may change (i.e., the ratio of signal from the holes to the cover plate changes) when repeating the experiment. However, the amount of cavity radiation, which is studied by this experiment, is not changed.

5.5.4 Emissivities and Leslie Cube

The angular dependence of emissivity can be seen in Figures 5.45 and 5.46. In Figure 5.45 the aluminum cubes with high emissivity black paint (Figure 4.17) are depicted. The top face of the cubes is observed for a much larger angle than the side faces. Therefore, according to Figures 1.32 and 1.33, the emissivity is lower

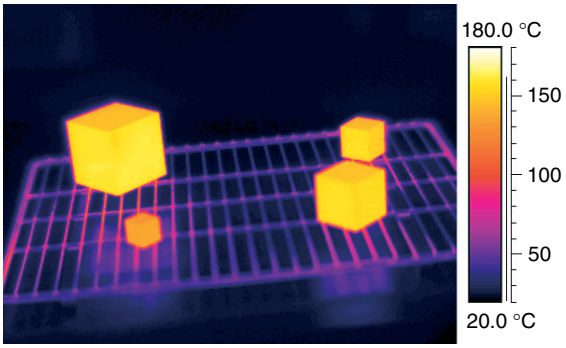

Figure 5.45 The normal emissivities of the faces of paint-covered metal cubes are the same. The two observable side faces are viewed from the same angle of about 45°, whereas the top face is seen from a larger angle. Owing to the angular dependence of emissivity, this leads to an apparently colder top face.

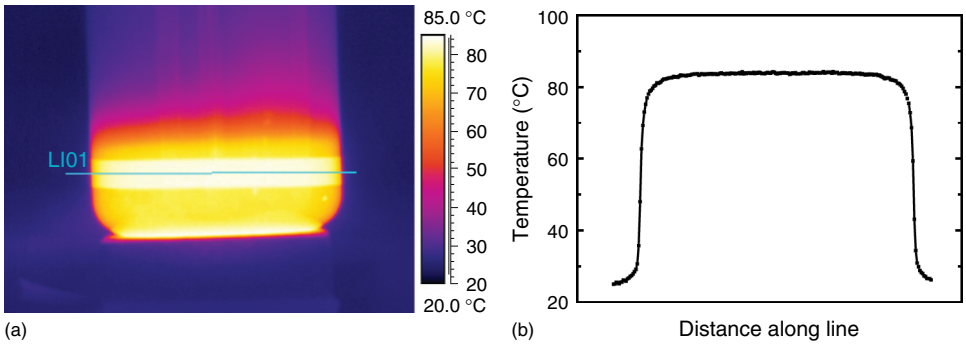

Figure 5.46 Glass cylinders filled with hot water allow to simultaneously observe emissivity effects due to a large variety of viewing angles. (a) IR image with line across a high emissivity tape. (b) Temperature profile along the line.

than for the side faces. As a result, the face appears to be cooler although it has the same temperature.

Figure 5.46 depicts a cylindrical container (large glass beaker) with an attached tape of high emissivity. One can clearly see that close to the edge, where the viewing angle is much larger, the apparent temperature drops with respect to the near normal observed areas of the object. A detailed analysis of the shape of the temperature profile is in agreement with the predictions of the drop of emissivity with observation angle (Figure 1.32).

Figure 5.47 shows an empty Leslie cube observed such that two side faces and the bottom face are all viewed from about the same viewing angle. If hot objects (finger of person) are close by, thermal reflections are clearly observable, which are dominant for the polished Cu metal surface and still detectable for the white and black paint covered surfaces.

The same Leslie cube is shown in Figure 5.48 while and after being filled with hot water. Now the surfaces are much hotter than the surroundings and no additional warm objects are around. Therefore, no thermal reflections are seen and the differences directly reflect the different surface emissivities at this fixed angle. The white and black paint surfaces show nearly the same emissivity for the LW camera, whereas the polished copper has still a lower emissivity compared to the diffusely scattering rough copper surface.

5.5.5
From Absorption to Emission of Cavity Radiation

In most experimental conditions in thermal physics, one has to deal with nonequilibrium conditions. An instructive experiment uses a small cavity, which resembles some kind of blackbody radiator. Such cavities are, for example, small graphite cylinders with an additional hole in the center of the side. Let us assume that the graphite surface may have an emissivity of say $\varepsilon = 0.9$, whereas the hole has a slightly larger

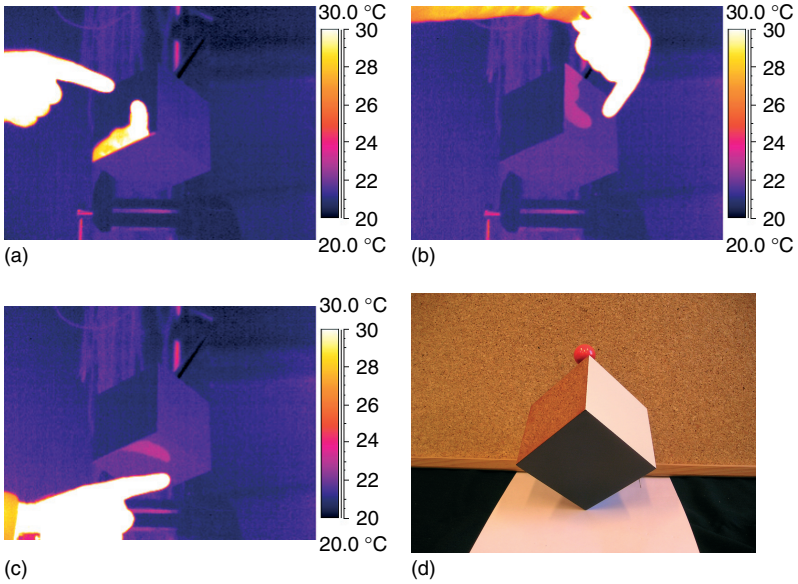

Figure 5.47 Empty Leslie cube with thermal reflections observed from an angle such that the sides (polished Cu, (a) white paint, (b) and black paint (c)) are viewed at the same angle.

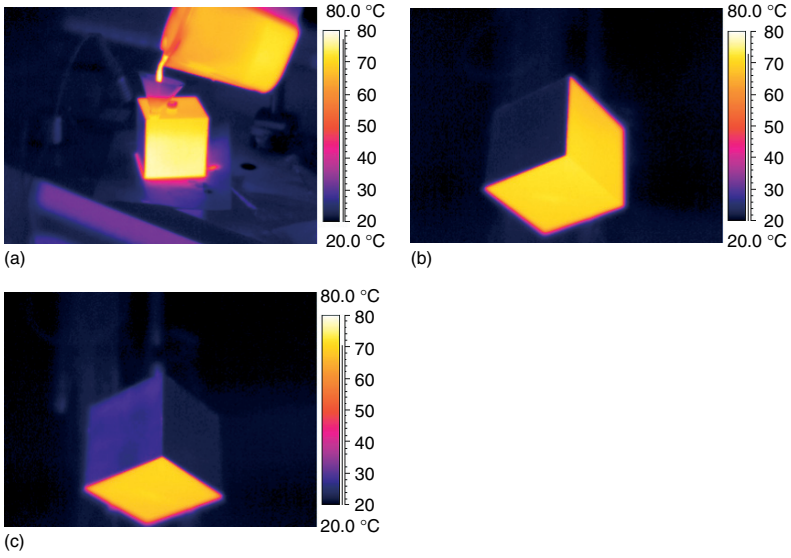

Figure 5.48 (a) Leslie cube filled with hot water and observed from an angle such that the sides are viewed at the same angle. (b) Polished Cu, white paint, and black paint (lowest segment). (c) Rough copper, polished copper, and black paint surface.

emissivity of, for example, around 0.98 (the exact values do not really matter, just the difference between surface and cavity values). Such graphite tubes are standard sample holders in atomic absorption spectroscopy (AAS). It is easily possible to heat the cavity by holding the end between fingers ($T > 30\,^{\circ}C$). After a dynamic thermal equilibrium between fingers and cavity is established, it is warmer than the surrounding, that is, the cavity is now not in thermal equilibrium with the colder surroundings. According to the laws of radiation, the temperature difference between cavity and surroundings will lead to a net emission of thermal radiation from the cavity, the amount being characterized by the emissivity. Since the cavity has a higher value of emissivity, it emits more radiation as clearly shown in Figure 5.49a.

The situation may, however, also be reversed by cooling the cavity. This was done by placing it between two ice cubes. After a (dynamic) thermal equilibrium between ice cube and cavity is established, the cavity is now much colder than the surrounding at room temperature. The cavity itself has high emissivity, that is, also high absorptivity (according to Kirchhoff's law). Therefore, it will absorb more radiation from the surrounding than the surface of the graphite tube. This energy quickly flows away to the ice cubes due to conduction, that is, we assume

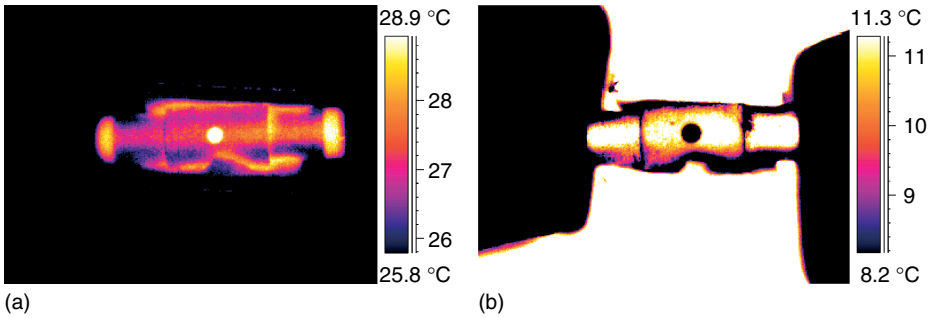

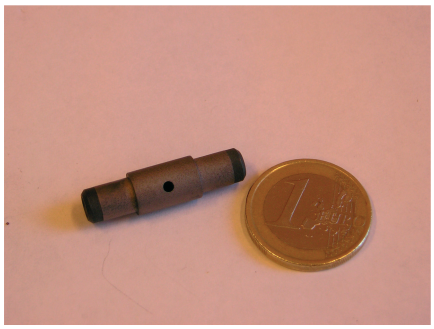
(c)

Figure 5.49 (c) Graphite tube (length = 3 cm, inner diameter 4 mm) with a small hole (diameter = 2 mm), typically used as sample holder in atom absorption spectroscopy (AAS) may serve as cavity. It can be used to record IR images while studying the transition from emission (a) to absorption (b). The tube can be heated by holding its ends between fingers (a) or cooled (b) by attaching the ends to ice cubes.

that the cavity temperature will stay low (this is why we speak of a dynamic equilibrium). The cavity will therefore emit radiation according to the cavity temperature, which is lower than the one of the surrounding. This has to be compared with the radiation from the graphite tube surface. Assuming the same temperature (thermal equilibrium within the tube) it should be lower than the one of the cavity due to the lower emissivity. However, since its emissivity is lower, its reflection coefficient is automatically much higher (Eq. (1.31)). Therefore the amount of thermal radiation from the much warmer surroundings, which will be reflected from the tube surfaces, add up to the pure thermal emission. This leads to a much larger total emission from the surface compared to the cavity. As a consequence, the cavity emits much less radiation than the tube surface as shown in Figure 5.49b.

5.5.6
Selective Absorption and Emission of Gases

The transition from absorption to emission of radiation by a selective emitter can also be demonstrated very nicely using selectively absorbing and emitting objects like molecular gases (for details see Chapter 7), Figure 5.50 depicts experimental results recorded with a LW camera using SF_6 [26]. SF_6 was filled in a plastic bag and cooled down to about $-20\,^{\circ}C$ in an air convection cooler. The cold gas was taken out of the cooler, the valve of the bag was opened and cold gas pressed out of the valve. The process was observed with the IR camera using the wall at room temperature as background. As shown in Figure 5.50a, the IR radiation from the wall toward the camera is significantly attenuated due to absorption within the gas. This is due to the strong absorption bands of SF_6 in the wavelength range around 10–11 μm.

In order to observe emission at these wavelengths, we placed the gas-filled bag in our air convection heating system. The gas was heated to about $80\,^{\circ}C$. It was taken out of the heater, the valve was opened, the gas was pressed out of the valve,

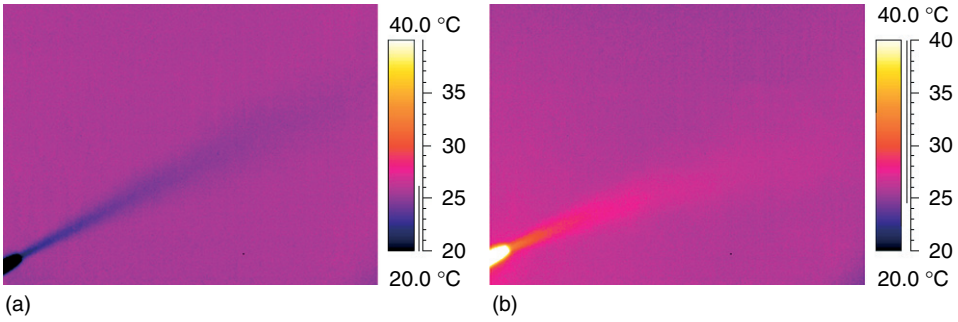

Figure 5.50 Absorption of cold SF_6 ($T \approx -20\,^{\circ}C$ (a)) and emission from warm SF_6 ($T \approx 80\,^{\circ}C$ (b)) in front of a wall at room temperature (detected with an LW camera).

and the process was again observed with the same wall at room temperature as background. The result of Figure 5.49b clearly demonstrates the emission of the hot gas, which leads to an increase of IR radiation from the streaming gas. Details of gas absorption and emission also with corresponding technological applications are discussed in Chapter 7.

References

1. Karstädt, D., Pinno, F., Möllmann, K.P., and Vollmer, M. (1999) Anschauliche Wärmelehre im Unterricht: ein Beitrag zur Visualisierung thermischer Vorgänge. *Prax. Naturwiss. Phys.*, **48** (5), 24–31.
2. Karstädt, D., Möllmann, K.P., Pinno, F., and Vollmer, M. (2001) There is more to see than eyes can detect: visualization of energy transfer processes and the laws of radiation for physics education. *Phys. Teach.*, **39**, 371–376.
3. Möllmann, K.-P. and Vollmer, M. (2000) Eine etwas andere, physikalische Sehweise – Visualisierung von Energieumwandlungen und Strahlungsphysik für die. *Phys. Bl.*, **56**, 65–69.
4. Möllmann, K.-P. and Vollmer, M. (2007) Infrared thermal imaging as a tool in university physics education. *Eur. J. Phys.*, **28**, S37–S50.
5. Halliday, D., Resnick, R., and Walker, J. (2001) *Fundamentals of Physics, Extended*, 6th edn, John & Wiley Sons, Inc.
6. Tipler, P.A. and Mosca, G. (2003) *Physics for Scientists and Engineers*, 5th edn, Freeman.
7. Bloomfield, L. (2007) *How Everything Works*, John Wiley & Sons, Inc.
8. Bellemans, A. (1981) Power demand in walking and pace optimization. *Am. J. Phys.*, **49**, 25–27.
9. Keller, J.B. (1973) A theory of competitive running. *Phys. Today*, **26**, 42–47.
10. Alexandrov, I. and Lucht, P. (1981) Physics of sprinting. *Am. J. Phys.*, **49**, 254–257.
11. Maroto, J.A., Pérez-Muñuzuri, V., and Romero-Cano, M.S. (2007) Introductory analysis of the Bénard Marangoni convection. *Eur. J. Phys.*, **28**, 311–320.
12. Consumer Energy Center of the California Energy Commission *http://www.consumerenergycenter.org/home/heating_cooling/evaporative.html*. (2010).
13. Planinsic, G. and Vollmer, M. (2008) The surface-to-volume-ratio in thermal physics: from cheese cubes to animal metabolism. *Eur. J. Phys.*, **29**, 369–384 and 661.
14. Vollmer, M. (2004) Physics of the microwave oven. *Phys. Educ.*, **39**, 74–81.
15. Baylie, M., Ford, P.J., Mathlin, G.P., and Palmer, C. (2009) The jumping ring experiment. *Phys. Educ.*, **44** (1), 27–32.
16. Bostock-Smith, J.M. (2008) The jumping ring and Lenz's law – an analysis. *Phys. Educ.*, **43** (3), 265–269.
17. Michalski, L., Eckersdorf, K., Kucharski, J., and McGhee, J. (2001) *Temperature Measurement*, 2nd edn, John Wiley & Sons, Ltd, Chichester.
18. Thuery, J. (1992) *Microwaves, Industrial, Scientific and Medical Applications*, Artech House, Boston.
19. Smith, B.L. and Carpentier, M.-H. (1993) *The Microwave Engineering Handbook*, vols. 1-3, Chapman & Hall, London.
20. Parker, K. and Vollmer, M. (2004) Bad food and good physics: the development of domestic microwave cookery. *Phys. Educ.*, **39**, 82–90.
21. Vollmer, M., Möllmann, K.-P., and Karstädt, D. (2004) More experiments with microwave ovens. *Phys. Educ.*, **39**, 346–351.
22. Vollmer, M., Möllmann, K.-P., and Karstädt, D. (2004) Microwave oven experiments with metals and light sources. *Phys. Educ.*, **39**, 500–508.
23. Vollmer, M., Möllmann, K.-P., and Pinno, F. (2007) Looking through matter: quantitative IR imaging when

observing through IR windows. Inframation 2007, Proceedings vol. 8, pp. 109–127.

24. Henke, S., Karstädt, D., Möllmann, K.P., Pinno, F., and Vollmer, M. (2004) in *Inframation Proceedings*, vol. 5 (eds R. Madding and G. Orlove), ITC, North Billerica, pp. 287–298.
25. Wolfe, W.L. and Zissis, G.J. (eds) (1993) *The Infrared Handbook*, revised edition, 4th printing, The Infrared Information Analysis Center, Environmental Research Institute of Michigan, Michigan.
26. Vollmer, M., Karstädt, D., Möllmann, K.-P., and Pinno, F. (2006) Influence of gaseous species on thermal infrared imaging. Inframation 2006, Proceedings vol. 7, pp. 65–78.